© 2022. Published by The Company of Biologists Ltd | Journal of Cell Science (2022) 135, jcs259514. doi:10.1242/jcs.259514

RESEARCH ARTICLE

DYRK2 maintains genome stability via neddylation of cullins in response to DNA damage

Akira Kawamura[1,*], Saishu Yoshida[1,*], Katsuhiko Aoki[1], Yuya Shimoyama[1,2], Kohji Yamada[1] and Kiyotsugu Yoshida[1,‡]

ABSTRACT

Neural precursor cell-expressed developmentally down-regulated 8 (NEDD8), an ubiquitin-like protein, is an essential regulator of the DNA damage response. Numerous studies have shown that neddylation (conjugation of NEDD8 to target proteins) dysfunction causes several human diseases, such as cancer. Hence clarifying the regulatory mechanism of neddylation could provide insight into the mechanism of genome stability underlying the DNA damage response (DDR) and carcinogenesis. Here, we demonstrate that dual-specificity tyrosine-regulated kinase 2 (DYRK2) is a novel regulator of neddylation and maintains genome stability. Deletion of DYRK2 leads to persistent DNA double-strand breaks (DSBs) and subsequent genome instability. Mechanistically, DYRK2 promotes neddylation through forming a complex with NAE1, which is a component of NEDD8-activating enzyme E1, and maintaining its protein level by suppressing polyubiquitylation. The present study is the first to demonstrate that DYRK2 controls neddylation and is necessary for maintaining genome stability.

This article has an associated First Person interview with the first author of the paper.

KEY WORDS: DYRK2, Genome stability, NEDD8, Neddylation, DNA damage response, DNA double-strand breaks

INTRODUCTION

DNA is constantly exposed to endogenous and exogenous factors, such as ultraviolet light, oxidative stress, carcinogens and radiation. To maintain genome stability, cells construct cellular pathways, including pathways for sensing, signaling and repair of damaged DNA, which are collectively termed the DNA damage response (DDR) (Ciccia and Elledge, 2010; Jackson and Bartek, 2009). The DDR is orchestrated by kinases that belong to the phosphoinositide 3-kinase (PI3K)-like kinase family, namely ataxia-telangiectasia mutated (ATM), ATM- and Rad3-related (ATR) and DNA-dependent protein kinase catalytic subunit (DNA-PKcs; encoded by *PRKDC*). These kinases induce the phosphorylation of histone H2A.X on serine 139 (known as γH2A.X), which is a critical early step in the cellular response to double-strand breaks (DSBs) (Rogakou et al., 1998) and which activates DNA repair signaling factors, such as p53 (encoded by *TP53*), resulting in the cell cycle arrest in G1, senescence or apoptosis (Blackford and Jackson, 2017). More recently, abnormalities of DNA repair or sensing processes or both have been found to induce genome instability and to lead to micronuclei (Takahashi et al., 2017; 2018). Notably, genome instability induces several disease processes, such as carcinogenesis (Aparicio et al., 2014), and is a factor in neurodegenerative diseases (McKinnon, 2017) and aging (Wang and Lindahl, 2016).

For the DDR, post-translational modifications (PTMs) are essential regulators (Walsh et al., 2005). Ubiquitin and the small ubiquitin-like modifier proteins (SUMOs), which are ubiquitin-like proteins (UBLs), have been well studied as regulators for the cellular response to DSBs (Schwertman et al., 2016). It is also known that other UBLs, especially neural precursor cell-expressed developmentally down-regulated 8 (NEDD8), have a role in this process. Neddylation is a type of PTM that conjugates UBLs and NEDD8 onto substrates. In the process of neddylation, NEDD8 is first activated by the NEDD8-activating enzyme E1 (a heterodimer composed of NAE1 and ubiquitin-like modifier activating enzyme 3; UBA3); the activated NEDD8 is then transferred to NEDD8-conjugating enzyme E2 [UBC12 (also known as UBE2M) or UBE2F]. Finally, NEDD8-conjugating enzyme E2 interacts with the substrate-specific NEDD8-E3 ligase to conjugate NEDD8 to its target substrates, mainly cullins, which are a large family of multiunit E3 ubiquitin ligases that regulate degradation of ∼20% of proteasome-regulated proteins (Petroski and Deshaies, 2005; Soucy et al., 2009). In the process of DSB repair, NEDD8 is accumulated at DNA damage sites (Ma et al., 2013). Moreover, inhibition of neddylation hypersensitizes human cells to DNA damaging agents, such as mitomycin C, cisplatin and ionizing radiation (Brown and Jackson, 2015). Hence, clarifying the regulatory mechanism of neddylation could provide insight into the genome stability underlying the DDR.

Dual-specificity tyrosine-regulated kinases (DYRKs) are a family that belongs to the CMGC group, which includes cyclin-dependent kinases (CDKs), mitogen-activated protein kinase (MAPKs), glycogen synthase kinases (GSKs) and CDK-like kinases (CLKs) (Becker and Sippl, 2011). In human cancer cells, we have identified DYRK2 as a regulator of p53-induced apoptosis in response to DNA damage (Taira et al., 2007) and of G1/S transition (Taira et al., 2012). Numerous studies have demonstrated that DYRK2 is downregulated in various tumors, such as tumors of the breast (Mimoto et al., 2017), colon (Ito et al., 2017; Kumamoto et al., 2020), brain (Shen et al., 2017), liver (Yokoyama-Mashima et al., 2019), lung (Yamashita et al., 2009a,b) and prostate (Taira et al., 2012). Importantly, this low DYRK2 expression is correlated with a poor prognosis (Enomoto et al., 2014; Mimoto et al., 2017; Taira et al., 2012; Zhang et al., 2016; Yoshida and Yoshida, 2019), indicating the tumor-suppressive functions of DYRK2. More recently, in normal cells, but not in tumor cells, whole-genome RNA sequencing of primary mouse embryonic

[1]Department of Biochemistry, The Jikei University School of Medicine, Tokyo, 105-8461, Japan. [2]Department of Surgery, The Jikei University School of Medicine, Tokyo, 105-8461, Japan.
*These authors contributed equally to this work

‡Author for correspondence (kyoshida@jikei.ac.jp)

A.K., 0000-0002-9914-7306; S.Y., 0000-0002-2574-6410; K.Y., 0000-0003-3108-7383

Handling Editor: David Glover
Received 26 October 2021; Accepted 3 May 2022

Journal of Cell Science (2022) 135, jcs259514. doi:10.1242/jcs.259514

fibroblasts (MEFs) derived from *Dyrk2*$^{-/-}$ mice has shown that these cells exhibit downregulation of genes related to cell division and the mitotic cell cycle checkpoint (Yoshida et al., 2020). These findings led us to speculate that DYRK2 plays other important roles in maintaining the homeostasis of normal cells and suppressing tumorigenesis.

In the present study, we investigated the role of DYRK2 in genome stability. Here, we demonstrate that DYRK2 is a novel regulator of neddylation and that is acts to maintains genome stability.

RESULTS

DYRK2 is required for genome stability

To investigate the involvement of DYRK2 in genome stability, we perform immuno-cytostaining for γH2A.X (phospho-histone variant H2A.X at Ser139), which is the earliest response marker of DSBs (Branzei and Foiani, 2008), in primary MEFs derived from wild-type and *Dyrk2*$^{-/-}$ mice (Yoshida et al., 2020). Higher levels of γH2A.X foci were observed in *Dyrk2*$^{-/-}$ MEFs (Fig. 1A,B). To validate whether this genome instability observed in *Dyrk2*$^{-/-}$ MEFs is conserved in other cell types, we knocked out *DYRK2* in immortalized human retinal pigment epithelia (hTRET-RPE1) cells by CRISPR/Cas9 technology (Katoh et al., 2017). Knockout of *DYRK2* (*DYRK2*$^{-/-}$) in hTRET-RPE1 cells also caused a marked increase of γH2A.X foci (Fig. 1C,D).

DSBs trigger the activation of the ATM–cell cycle checkpoint kinase 2 (CHK2; also known as CHEK2) pathway, which is one of the major DDR pathways (Ahn et al., 2000, 2002). Deletion of *DYRK2* showed no effects on total ATM and CHK2, but significantly promoted phosphorylation of ATM (Ser1981) and CHK2 (Thr68) (Fig. 1E; Fig. S1). Persistent activation of the DDR causes micro-nuclei to form (Takahashi et al., 2018). Knockout of DYRK2 significantly induced formation of micro-nuclei in hTRET-RPE1 cells (Fig. 1F,G) and also in *Dyrk2*$^{-/-}$ MEFs (Fig. 1H,I). These data demonstrate that deletion of *DYRK2* induces genome instability via persistent DSBs and activation of the ATM–CHK2 pathway.

DYRK2 depletion causes G0/1 phase cell cycle arrest and induces cellular senescence

The activation of the DDR orchestrates the detection and repair of DNA damage with transient cell cycle arrest to ensure maintenance of genome stability and also induce senescence or apoptosis (Jackson and Bartek, 2009). To investigate the effects of DYRK2 in cell cycle, hTRET-RPE1 cells were synchronized at G0 phase by serum starvation for 24 h and then re-addition of serum (Fig. 2A). Cells progressed to the S-G2-M phase over time after serum had been added back. A transient knockdown by means of siRNA against *DYRK2* (si*DYRK2*), however, induced a delay in cell cycle re-entry (Fig. 2B,C). The protein level of G1/S markers [cyclin D1 and p27 (encoded by *CDKN1B*)] also showed that there was a delay in cell cycle re-entry in hTRET-RPE1 cells (Fig. 2D). Cells undergoing senescence show cell cycle arrest concurrently with metabolic changes, including production of senescence-associated β-galactosidase (SA-β-gal) (Coppé et al., 2008). Under serum starvation, the proportion of SA-β-gal-positive cells was significantly higher in *DYRK2*$^{-/-}$ hTRET-RPE1 cells than in wild-type cells (Fig. 2E,F). Similar results were observed in *Dyrk2*$^{-/-}$ MEFs (Fig. 2G). Taken together, these results demonstrate that depletion of DYRK2 induces G0/1 phase cell cycle arrest and initiation of cellular senescence.

DYRK2 depletion induces p21 and p38 MAPK via stabilization and activation of p53

To elucidate the molecular mechanisms of G0/1 phase cell cycle arrest and initiation of cellular senescence caused by genome instability, we focused on factors involved in cellular stress and cell cycle arrest. Especially, we investigated the relationship between DYRK2 and the DDR factor p53, which is activated via stabilization and translocation to nuclei by cellular stress, including DSBs (Branzei and Foiani, 2008; Hafner et al., 2019). We found that protein levels of p53 and its downstream factor, p21, were increased (Fig. 3A,B) and accumulated in nuclei in *DYRK2*$^{-/-}$ hTRET-RPE1 (Fig. 3C). Gene expression of *CDKN1A* (encoding p21) was upregulated in *DYRK2*$^{-/-}$ hTRET-RPE1 cells (Fig. S2A). Phosphorylation of p38 MAPKs, which respond to cellular stress and link to the cell cycle through senescence and differentiation (Yee et al., 2004), was also increased in *DYRK2*$^{-/-}$ hTRET-RPE1 cells (Fig. 3A). Similar phenotypes were observed in *Dyrk2*$^{-/-}$ MEFs (Fig. S2B,C) and a transient knockdown by means of si*DYRK2* in hTRET-RPE1 cells (Fig. S2D). Under basal conditions, the protein level of p53 is maintained at low levels because it is degraded rapidly following ubiquitylation by the associated ubiquitin ligase, MDM2 (Shieh et al., 1997; Siliciano et al., 1997). Under stress conditions, however, p53 is stabilized by phosphorylation at Ser15, which prevents the recruitment of MDM2. The protein level of phospho-p53 (Ser15) was increased in *DYRK2*$^{-/-}$ hTRET-RPE1 cells (Fig. 3D) indicating that stabilization of p53 is, at least in part, caused by inhibition of interaction with MDM2.

We subsequently confirmed whether p53 regulates p21 and p38 MAPKs. The expression of p21 is regulated at the transcription level by direct p53 binding to p53 response elements in the promoter of the p21 gene (Abbas and Dutta, 2009). Transient knockdown by means of siRNA against *TP53* (siTP53) repressed protein levels of p21 and p38 MAPKs in *DYRK2*$^{-/-}$ hTRET-RPE1 cells (Fig. 3E). In contrast, protein levels of p53 and p21 remained unchanged upon treatment with SB203580 (a p38 MAPK inhibitor) in *DYRK2*$^{-/-}$ hTRET-RPE1 cells (Fig. S2E). Collectively, these data show that the deletion of *DYRK2* induces p53 stabilization and activation to induce p21 transcription and p38 MAPK activation.

DYRK2 promotes neddylation through NAE1

To investigate how DYRK2 suppresses persistent DSBs, we focused on protein neddylation, which plays important roles during DNA damage signaling (Ma et al., 2013; Wang et al., 2017). We found that protein levels of NAE1 and UBA3, which compose the E1 enzyme in this process (see Introduction), were decreased in *DYRK2*$^{-/-}$ hTRET-RPE1 cells (Fig. 4A). Gene expression analysis demonstrated no changes in the gene expression levels of *NAE1* and *UBA3* in *DYRK2*$^{-/-}$ hTRET-RPE1 cells (Fig. S3). These data indicate that the deletion of *DYRK2* reduces the stabilization of NAE1 and UBA3 in a posttranslational manner. Notably, NEDD8–cullins (neddylated cullins) were suppressed in *DYRK2*$^{-/-}$ hTRET-RPE1 cells (Fig. 4A). To verify that DYRK2 is involved in the stabilization of NAE1 and UBA3, we conducted a transient overexpression experiment with wild-type human DYRK2 or a DYRK2-K251R construct, which expresses a kinase dead mutant (Taira et al., 2012) in *DYRK2*$^{-/-}$ hTRET-RPE1 cells by adenovirus infection (Yokoyama-Mashima et al., 2019; Yoshida et al., 2020). Overexpression of the wild-type *DYRK2* construct, but not the *DYRK2-K251R* mutant, restored protein levels of NAE1, UBA3 and NEDD8–cullins (Fig. 4B).

To understand the mechanisms underlying the suppression of E1 ligases in *DYRK2*$^{-/-}$ hTRET-RPE1 cells, we analyzed protein–protein interaction between DYRK2 and the E1 enzyme by immunoprecipitation. The result demonstrates that DYRK2 interacts with NAE1 but not with UBA3 (Fig. 4C). The DYRK2-K251R mutant also interacted with NAE1; however, this interaction was markedly less compared to that of wild-type DYRK2 (Fig. S4).

Journal of Cell Science (2022) 135, jcs259514. doi:10.1242/jcs.259514

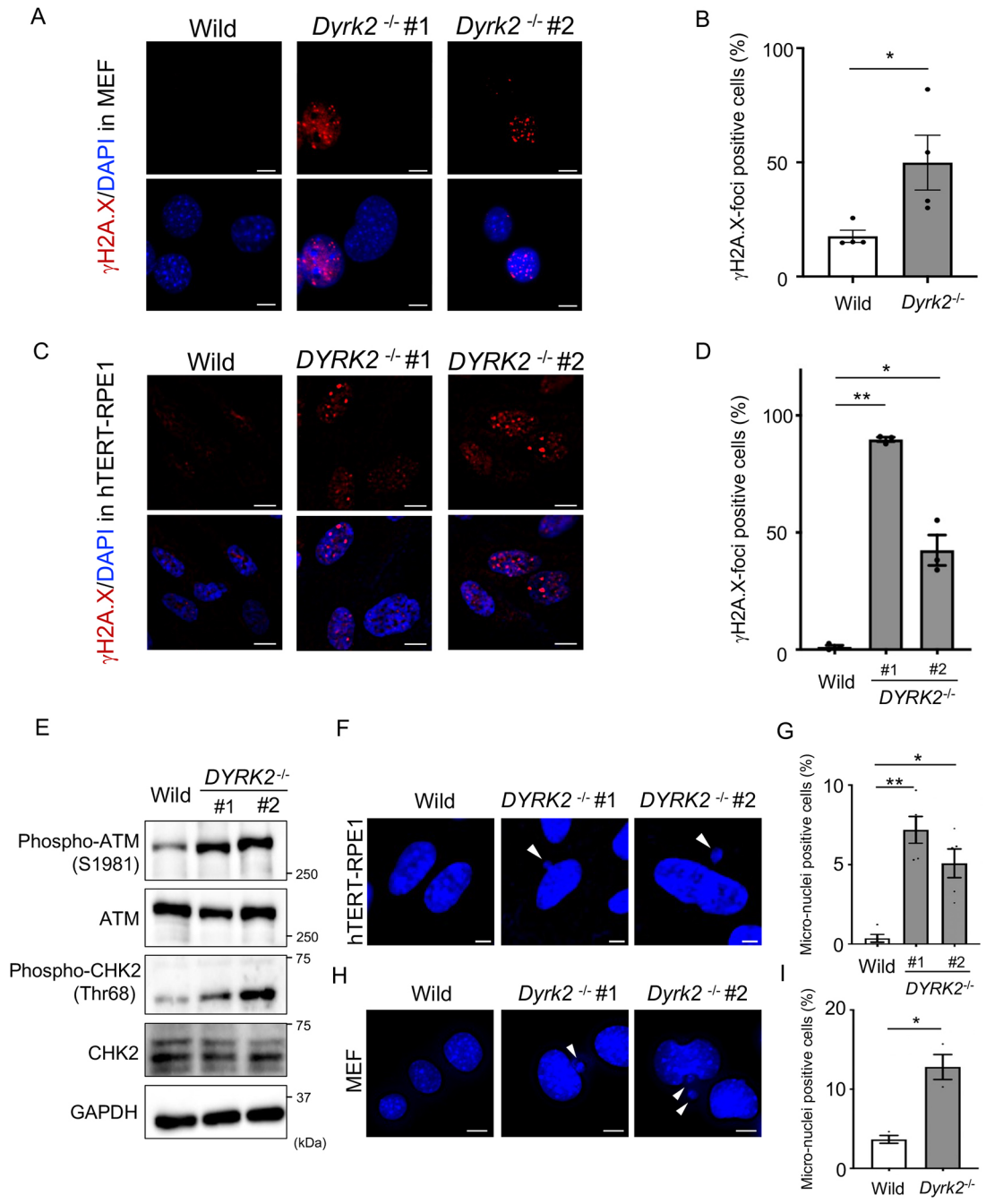

Fig. 1. DYRK2 depletion induces genome instability via DSBs and activation of the ATM-CHK2 pathway. (A,B) Wild-type and *Dyrk2*$^{-/-}$ primary MEFs were immunocytostained for γH2A.X (red). Nuclei were stained with DAPI (blue). Scale bars: 10 µm. The proportion of γH2A.X-foci-positive cells with more than five foci is shown (B). Data are presented as the means±s.e.m. (*n*=4 biological replicates per condition). (C,D) Wild-type and *DYRK2*$^{-/-}$ hTERT-RPE1 cells were immunocytostained for γH2A.X (red). Nuclei were stained with DAPI (blue). Scale bars: 5 µm. The proportion of γH2A.X-foci-positive cells with more than five foci is shown (D). Data are presented as the means±s.e.m. (*n*=3 technical replicates per condition). (E) Protein levels of phospho-ATM (S1981), ATM, phospho-CHK2 (Thr68), and CHK2 in wild-type and *DYRK2*$^{-/-}$ hTERT-RPE1 cells were measured by immunoblotting. GAPDH serves as a loading control. Blot shown is representative of at least three repeats. (F,G) Detection of the micro-nuclei in the cytoplasm in *DYRK2*$^{-/-}$ hTERT-RPE1 cells. Wild-type and *DYRK2*$^{-/-}$ hTERT-RPE1 cells were stained for DAPI (blue). Arrowheads indicate a micro-nucleus in the cytoplasm. Scale bars: 5 µm. The proportion of micro-nuclei is shown (G). Data are presented as the means±s.e.m. (*n*=4 technical replicates per condition). (H,I) Detection of micro-nuclei in the cytoplasm in *Dyrk2*$^{-/-}$ MEFs. Wild-type and *Dyrk2*$^{-/-}$ MEFs were stained for DAPI (blue). Arrowheads indicate micro-nuclei in the cytoplasm. Scale bars: 10 µm. The proportion of micro-nuclei is shown (I). Data are presented as the means±s.e.m. (*n*=3 biological replicates per condition). **P*<0.05, ***P*<0.01 (paired two-tailed Student's *t*-test in B,I; one-way ANOVA followed by Tukey's multiple comparison test in D,G).

Moreover, a transient knockdown by si*DYRK2* induced polyubiquitylation of NAE1 (Fig. 4D). These data indicate that DYRK2 stabilizes the E1 enzyme in a kinase-activity-dependent manner by binding to NAE1 and suppressing its ubiquitylation.

Finally, we examined whether overexpression of NAE1 and UBA3, which is suppressed in DYRK2$^{-/-}$ cells, restores genomic stability. In *DYRK2*$^{-/-}$ hTRET-RPE1 cells, immunocytostaining for γH2A.X demonstrated that NAE1 and UBA3 double-positive cells

Journal of Cell Science (2022) 135, jcs259514. doi:10.1242/jcs.259514

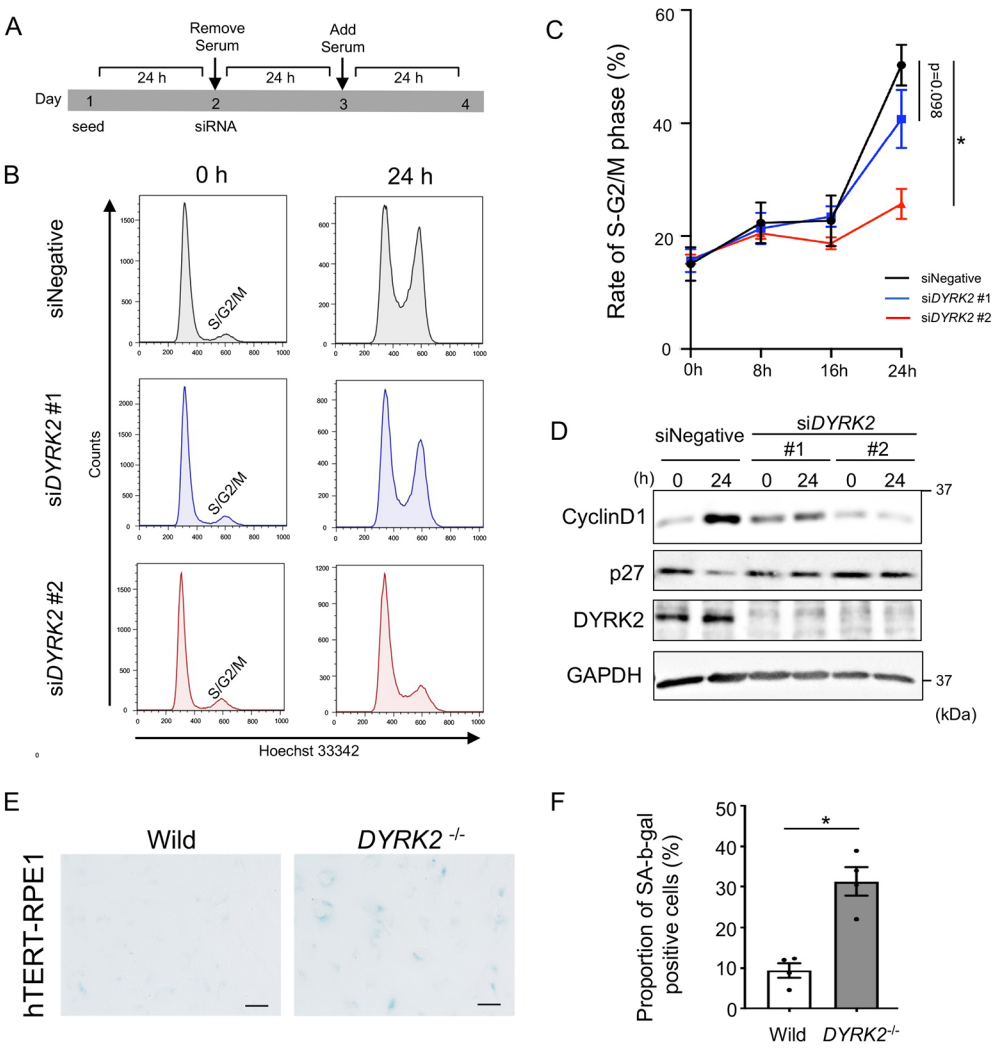

Fig. 2. DYRK2 depletion causes G0/1 phase cell cycle arrest and induces cellular senescence initiation. (A) Diagrams depicting the timeline of experiments. hTERT-RPE1 cells were synchronized in G0 phase by serum starvation for 24 h, followed by induction to re-enter the cell cycle by serum re-stimulation with nocodazole. (B,C) Cell cycle re-entry analysis by flow cytometry in hTERT-RPE1 cells treated with siNegative or two independent siRNAs for *DYRK2* (si*DYRK2*). Cells were analyzed at 0, 8, 16 and 24 h after serum re-stimulation. Data are presented as the means±s.e.m. (n=3 technical replicates per condition). *P<0.05 (one-way ANOVA followed by Tukey's multiple comparison test). (D) Protein level of cyclin D1 and p27 in *DYRK2*-knockdown hTERT-RPE1 cells. hTERT-RPE1 cells were treated with siNegative or two independent siRNAs for *DYRK2* for 0 or 24 h and analyzed by immunoblotting. GAPDH serves as a loading control. Blot shown is representative of at least three repeats. (E,F) Senescence-associated β-galactosidase (SA-β-gal) analysis of wild-type and *DYRK2* $^{-/-}$ hTRET-RPE1 cells. SA-β-gal staining on wild-type and *DYRK2*$^{-/-}$ hTRET-RPE1 cells (E). Scale bars: 50 µm. The proportion of SA-β-gal-positive cells was analyzed by flow cytometry (F). Data are presented as the means±s.e.m. (n=4 technical replicates per condition). *P<0.05 between wild-type and *DYRK2*$^{-/-}$ (paired two-tailed Student's t-test). (G) SA-β-gal analysis of wild-type and *Dyrk2*$^{-/-}$ MEFs. Images shown are representative of at least three repeats. Scale bars: 50 µm.

had decreased levels of γH2A.X foci (Fig. 4E,F). Taken together, these findings indicate that DYRK2 maintains the level of neddylation by binding to the E1 enzyme and contributes to the maintenance of genomic stability.

DISCUSSION

DYRK2 is a novel neddylation regulator

The present study demonstrates that the loss of DYRK2 suppresses neddylation and causes persistent DSBs and DDRs, such as cell cycle arrest and cellular senescence, through the activation of p21 and p38 MAPKs via p53 (Fig. 5). Mechanistically, DYRK2 promotes neddylation via forming a complex with NAE1 and maintains the protein levels of the E1 enzyme (Fig. 5). Ultimately, NEDD8 conjugates mainly with cullins and activates cullin–RING ligases (CRLs), which regulates ∼20% of the degradation of proteasome-regulated proteins and promotes DDR (Petroski and Deshaies, 2005; Soucy et al., 2009).

Recently, MLN4924, which is a selective small-molecular inhibitor of the NEDD8-activating enzyme, has been found to suppress E1 enzyme activity and the neddylation of cullins (Brownell et al., 2010). Treatment with MLN4924 causes accumulation of CRL substrates and DSB formation, which consequently induce persistent activation of DDRs and cellular senescence (Milhollen et al., 2011; Jia et al., 2011). Similarly, our present data indicate that deletion of DYRK2 shows this typical phenotype when neddylation is suppressed by treatment with MLN4924. Taken together with the finding that overexpression of NAE1 and UBA3 restores genome stability in *DYRK2*$^{-/-}$ cells, we conclude that DYRK2 contributes to genome stability via regulation of neddylation. To elucidate the function of DYRK2 in NAE1 stabilization, we focus on the ubiquitin-proteasome system. Deletion of DYRK2 promotes poly-ubiquitylation and decreases the protein level of NAE1, implying that DYRK2 stabilizes NAE1 through the inhibition of ubiquitylation and subsequent proteasomal degradation. Although mechanisms

Journal of Cell Science (2022) 135, jcs259514. doi:10.1242/jcs.259514

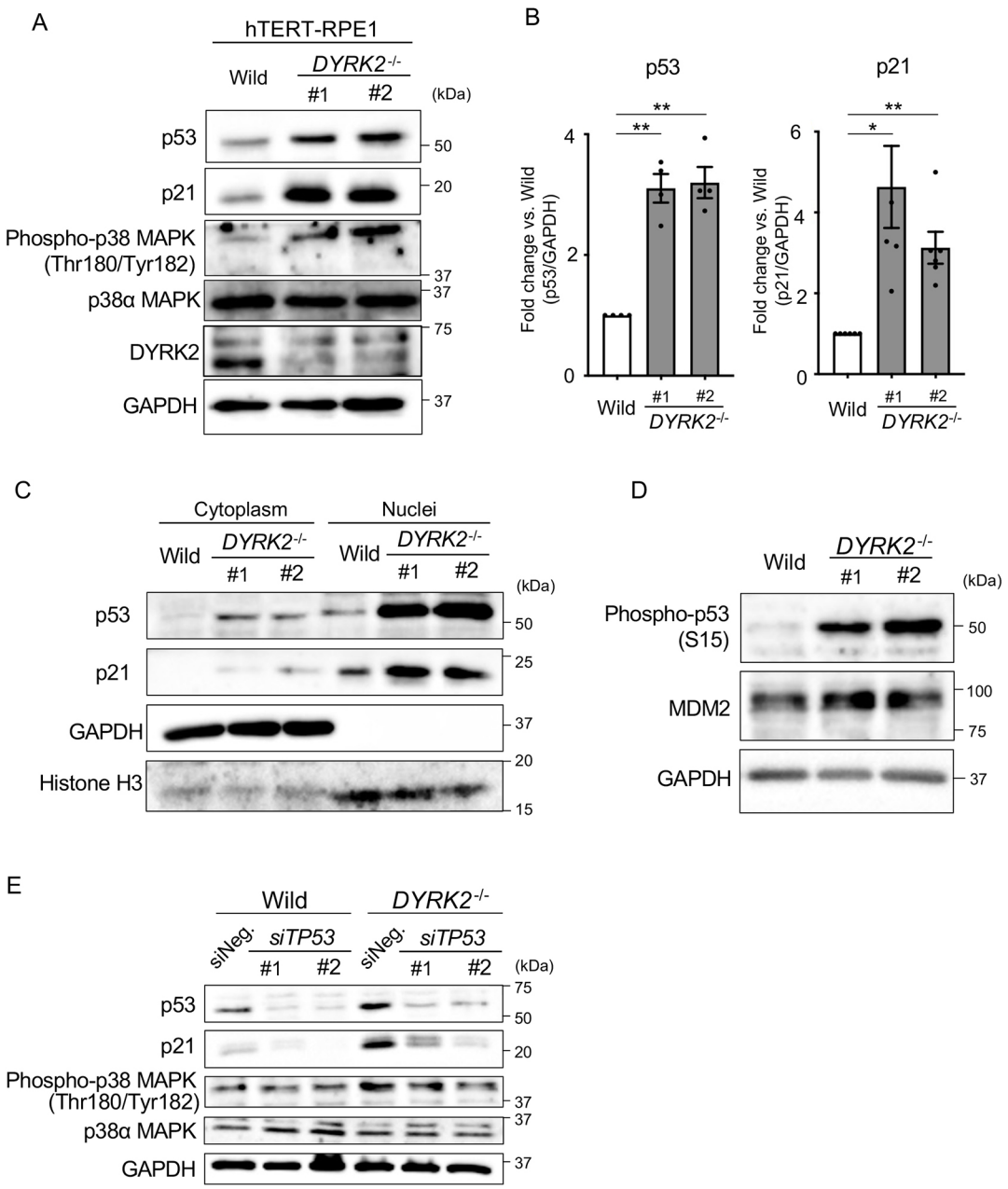

Fig. 3. DYRK2 depletion causes p21 and p38 MAPK activation via p53. (A,B) Protein levels of p53, p21, phospho-p38 MAPKs, p38α MAPK and DYRK2 in wild-type and two *DYRK2*$^{-/-}$ hTERT-RPE1 cell lines were measured by immunoblotting. Protein level as fold changes of p53 and p21 was calculated by comparing protein levels relative to those of wild-type hTERT-RPE1 cells in after normalization to the GAPDH loading control (B). Data are presented as the means±s.e.m. (n=4 and 6 technical replicates per condition, respectively). *P<0.05, **P<0.01 (one-way ANOVA followed by Tukey's multiple comparison test). (C) Protein levels of p53 and p21 in wild-type and two *DYRK2*$^{-/-}$ hTERT-RPE1 cell lines separated into cytoplasmic and nuclear fractions were measured by immunoblotting. GAPDH and histone H3 serve as loading controls. (D) Protein levels of phosphor-p53 (Ser15) and MDM2 in wild-type and *DYRK2*$^{-/-}$ hTERT-RPE1 cells were measured by immunoblotting. GAPDH serves as a loading control. (E) Protein levels of p53, p21, phospho-p38 MAPK, p38a MAPK, and DYRK2 in wild-type and *DYRK2*$^{-/-}$ hTERT-RPE1 cells treated with siNegative or two independent siRNAs against *TP53* (si*TP53*) were measured by immunoblotting. GAPDH serves as a loading control. Blots shown in C–E are representative of at least three repeats.

underlying the suppression of NAE1 ubiquitylation via interaction with DYRK2 in a kinase-dependent manner remain unclear, the present study is the first to demonstrate that the protein level of NAE1 is regulated by inhibition of polyubiquitylation.

Multiple functions of DYRK2 in the maintenance of cellular homeostasis

To protect against a variety of stresses, cells keep cellular homeostasis via cell arrest, senescence, and apoptosis (Childs et al., 2014). We have reported that ATM phosphorylates DYRK2 at Thr33 and Thr369 under DNA damage and that DYRK2 subsequently phosphorylates p53 at Ser46 to induce apoptosis (Taira et al., 2007). This induction of apoptosis contributes to the elimination of cells with irreparable DNA damage (Coates et al., 2005). DYRK2 also directly interacts with ring finger protein 8 (RNF8), which catalyzes Lys63-linked ubiquitylation of histone H2A.X in response to genotoxic stress (Yamamoto et al., 2017). Interestingly, DYRK2 directly phosphorylates telomerase reverse

Journal of Cell Science (2022) 135, jcs259514. doi:10.1242/jcs.259514

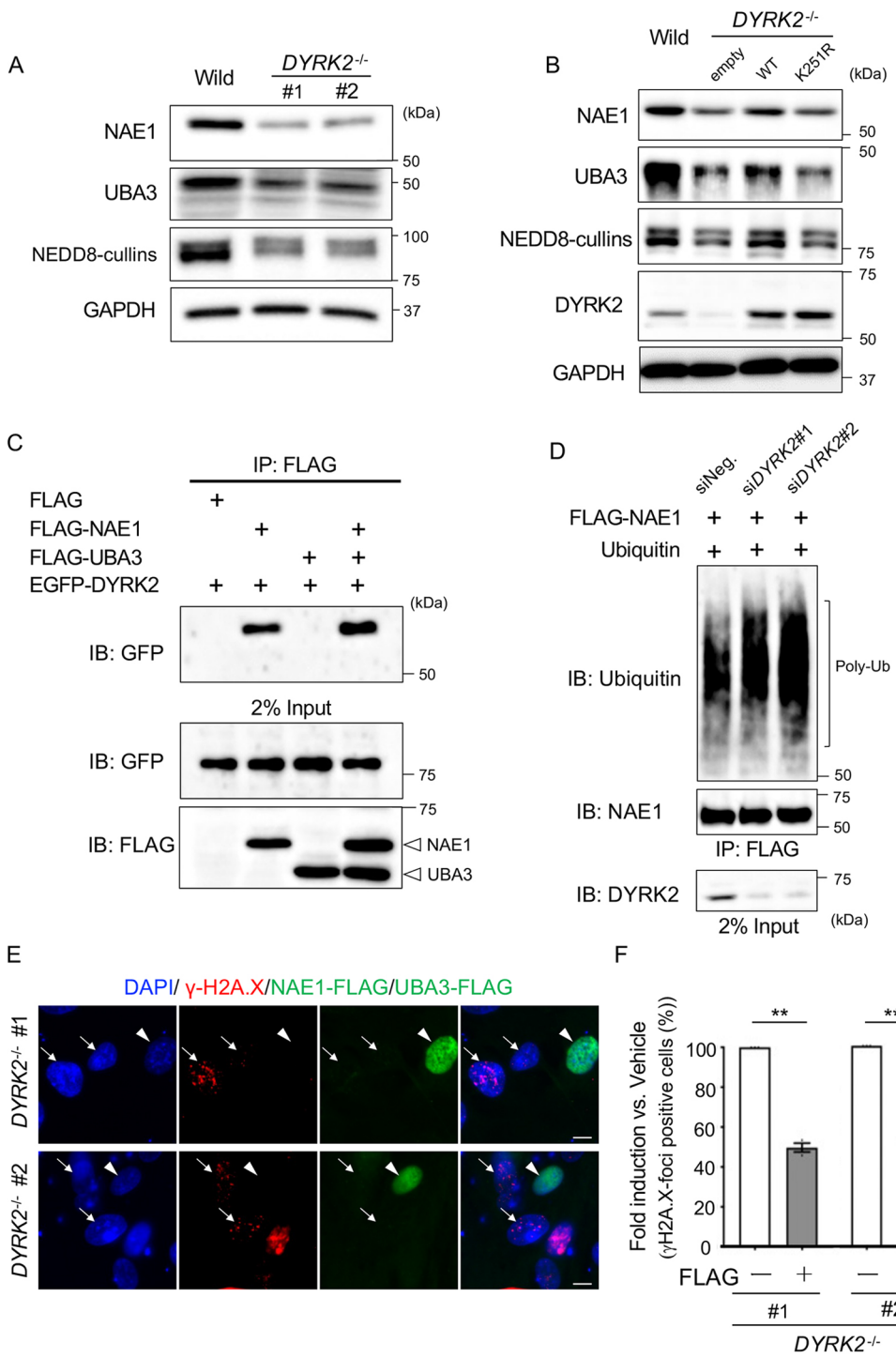

Fig. 4. DYRK2 promotes neddylation through NEDD8-activating enzyme E1. (A) Protein levels of NAE1, UBA3, and NEDD8–cullins (detected using anti-NEDD8 antibody) in wild-type and *DYRK2* $^{-/-}$ hTERT-RPE1 cells were measured by immunoblotting. GAPDH serves as a loading control. (B) Protein levels of NAE1, UBA3, and NEDD8–cullins and DYRK2 in wild-type and *DYRK2*$^{-/-}$ hTERT-RPE1 cells overexpressing *DYRK2* or *DYRK2-K251R* (kinase dead) constructs via adenovirus infection were measured by immunoblotting. GAPDH serves as a loading control. (C) Lysates from Lenti-X 293T cells co-transfected with an empty vector (pcDNA3-FLAG), FLAG–NAE1 and/or FLAG–UBA3 with EGFP–DYRK2 were immunoprecipitated with anti-Flag agarose. Immunoprecipitates and input were then subjected to immunoblot analysis with anti-GFP or anti-FLAG. (D) Lysates from Lenti-X 293T cells treated with siNegative or two independent siRNAs against DYRK2 (si*DYRK2*) and transfected with a FLAG–NAE1 and HA–Ubiquitin followed by treatment of MG-132 for 4 h were immunoprecipitated with anti-Flag agarose. Immunoprecipitates and input were then subjected to immunoblot analysis with anti-ubiquitin, anti-NAE1 and anti-DYRK2 antibodies. Blots shown in A–D are representative of at least three repeats. (E,F) Two independent *DYRK2*$^{-/-}$ hTERT-RPE1 cells lines transfected with FLAG–NAE1 and UBA3–FLAG vector (green) were immuno-cytostained for γH2A.X (red). Nuclei were stained with DAPI (blue). Arrowheads and arrows indicate FLAG-positive and -negative cells, respectively. Scale bars: 10 µm. The proportion (%) of γH2A.X-positive cells with more than five foci are shown (E). Each proportion was measured by counting at least 40 cells. Fold change was calculated by comparing the proportion of γH2A.X-positive cells from the FLAG-positive cells relative to those of FLAG-negative ones. Data are presented as the means±s.e.m. (n=3 technical replicates per condition). $^{**}P$<0.01 (paired two-tailed Student's t-test).

Journal of Cell Science (2022) 135, jcs259514. doi:10.1242/jcs.259514

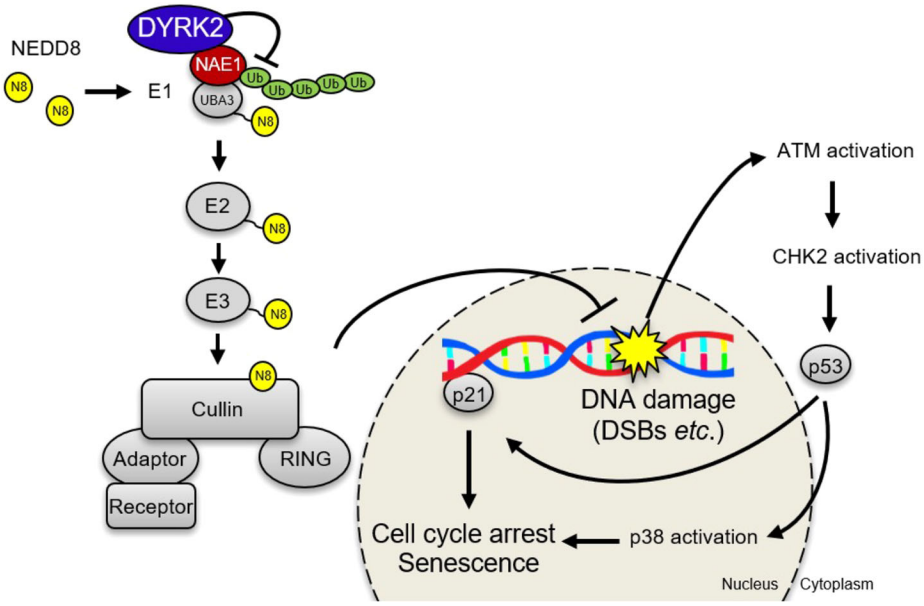

Fig. 5. Schematic representation of function of DYRK2 in neddylation and the DNA damage response. DYRK2 positively regulates neddylation through direct interacting to NAE1 for stabilization via inhibition of ubiquitylation, which is required for proteasomal degradation. In *DYRK2*-deletion cells, suppression of neddylation occurs because of decreased protein levels of E1 enzyme, which causes dysfunction of DNA repair and accumulation of DSBs. The DSBs induce activation of p21 and p38 MAPKs via p53, and eventually leads to G0/1 phase cell cycle arrest and initiation of cellular senescence.

transcriptase (TERT) and induces subsequent ubiquitylation and degradation as a scaffold for E3 isolated by the differential display (EDD; also known as UBR5)–DNA-damage binding protein 1 (DDB1)–Vpr-binding protein (VprBP; also known as DCAF1) (EDVP) E3 ligase complex (Jung et al., 2013). TERT, a component of telomerase, which adds a chromosomal end structure, contributes to genomic stability (Cech, 2004; Negrini et al., 2010). Taken together with the present finding that DYRK2 maintains genomic stability via neddylation, DYRK2 functions in cellular homeostasis in a multistep manner.

DYRK2 might suppress carcinogenesis via neddylation

Numerous studies indicate that neddylation dysfunction causes several human diseases (Zhang et al., 2021; Shukla et al., 2020; Jiang and Jia, 2015). Especially in cancers, the components of CRLs are overexpressed or mutated, and many CRLs regulate the activity of proteins that act as tumor suppressors or oncoproteins (Watson et al., 2011). In *TP53*-deficient hTERT-RPE1 cells, suppression of neddylation has recently been found to promote oncogenic proliferation and play an important role in tumorigenesis (Drainas et al., 2020). In this context, DYRK2 induces apoptosis via phosphorylation of p53 (Taira et al., 2007) and suppresses the cell cycle via oncogenic factors c-Jun and c-Myc (Taira et al., 2012). Given the findings that DYRK2 is downregulated in various cancer cells, DYRK2 plays a tumor-suppressive function (Enomoto et al., 2014; Mimoto et al., 2017; Taira et al., 2012; Zhang et al., 2016; Yoshida and Yoshida, 2019). In the present study, loss of DYRK2 induced γH2A.X foci, indicating genome instability via persistent DSBs. Genome instability via abnormalities of DNA repair or sensing processes, or both, induces carcinogenesis (Deman and Van Larebeke, 2001; Kinzler and Vogelstein, 1997; Loeb, 1994). Although the present study does not provide direct evidence that deletion of DYRK2 causes tumorigenesis, genome stabilization via DYRK2-mediated neddylation might contribute to the suppression of carcinogenesis.

Conclusion

The present study is the first to demonstrate that DYRK2 regulates neddylation and is necessary for maintaining genome stability. Mechanistically, DYRK2 promotes neddylation by forming a complex with NAE1 and maintains NAE1 protein levels by suppressing polyubiquitylation. These findings support further understanding of the maintenance of genomic stability and the mechanisms of the carcinogenesis suppression via neddylation.

MATERIALS AND METHODS

Plasmid constructs

Full-length cDNA fragments of human DYRK2, NAE1, UBA3 and ubiquitin were amplified by PCR and cloned in frame into pcDNA3+FLAG, pcDNA3+HA and pEGFP-C1 (Takara Bio Inc., Otsu, Japan) using NEBuilder HiFi DNA Assembly Master Mix (New England Biolabs, Ipswich, MA, USA). The nucleotide sequences of the primers used are listed in Table S1.

Cell culture and transfection

Cell culture was performed as described in a previous study (Yoshida et al., 2020). Primary MEFs were generated from wild-type and *Dyrk2*$^{-/-}$ mouse embryos at E13.5 (Yoshida et al., 2020). The MEFs and immortalized human retinal pigment epithelia cells (hTERT-RPE1, ATCC, Manassas, VA, USA) and the Lenti-X 293T cell line (Takara Bio Inc.) were cultured in Dulbecco's modified Eagle's medium (Nacalai Tesque, Kyoto, Japan) with 10% fetal bovine serum (Biowest, Nuaillé, France), 1% GultaMAX (Gibco, Gaithersburg, MD, USA), and 1% penicillin-streptomycin (Nacalai Tesque) at 37°C under 5% CO_2. For SB203580 stimulation, cells were treated with 0.5 µM SB203580 (Selleck Biotech, Tokyo, Japan) for 72 h after serum starvation. Transient knockdown was achieved with the Lipofectamine RNAiMAX transfection regent (Thermo Fisher Scientific, Waltham, MA, USA) according to the manufacturer's instructions with a final concentration of 20 nM siRNA (Table S2). For transient overexpression, transfection was performed with the reagent X-tremeGENE^{TM}9 (Merck KGaA, Darmstadt, Germany) for hTERT-RPE1 cells and with Polyethylenimine 'Max' (Polysciences, Warrington, PA, USA) for Lenti-X 293T cells. For MG-132 treatment, Lenti-X 293T cells were incubated with 5 µM MG-132 (Merck) for 4 h.

CRISPR/Cas9-mediated knockout in hTERT-RPE1 cells

CRISPR/Cas9-mediated *DYRK2* knockout hTERT-RPE1 cells were made using homology-independent repair performed according to a previous report (Katoh et al., 2017). Briefly, two independent single-guide RNA (sgRNA) sequences targeting the human *DYRK2* gene (#1: 5′-CCT-GGATCTGTCCGTGAGCG-3′) and (#2: 5′-GAGCCCGGTAAAAACGC-GAC-3′) were designed and inserted into peSpCAS9(1.1)-2×sgRNA (Addgene plasmid #80768). The hTERT-RPE1 cells were transfected

with the sgRNA vector and the pDonor-tBFP-NLS-Neo (Universal) donor knock-in vector (Addgene plasmid #80767) via a X-tremeGENE^{TM}9 transfection reagent (Roche Applied Science), selected by 600 µg/ml G418, and subcloned.

Adenovirus infection

Adenovirus construction and infection were performed as described in a previous study (Yoshida et al., 2020). Briefly, Flag–DYRK2 and Flag–DYRK2-K251R (Mimoto et al., 2013; Taira et al., 2010; Yokoyama-Mashima et al., 2019) were expressed depending upon Cre expression.

Immunocytochemistry

For immunocytochemistry, cells were cultured on eight-well chamber slides (Thermo Fisher Scientific) coated with Poly-D-lysin (Sigma-Aldrich, St Louis, MO, USA). Cells were fixed and antigen-retrieved depending on the antibody. The primary antibody reaction was performed at an appropriate dilution (Table S2) in the presence of a blocking buffer at 4°C overnight. After immunoreactions, cells were incubated with secondary antibodies via Cy3- or Cy5-conjugated AffiniPure donkey anti-mouse and rabbit IgG (Jackson ImmunoResearch, West Grove, PA, USA). The cells were then washed and incubated with DAPI (Vector Laboratories, Burlingame, CA, USA). Immunofluorescence was observed under a BZ-X800 fluorescence microscope (Keyence, Osaka, Japan).

Immunoblotting

Cells were washed twice in chilled phosphate-buffered saline and lysed with a RIPA buffer containing inhibitors (1 mM PMSF, 10 µg/ml aprotinin, 1 µg/ml leupeptin, 1 µg/ml pepstatin A, 1 mM Na_3VO_4, 10 mM NaF and 1 mM dithiothreitol). Equal amounts of protein (5 µg) were separated by SDS-PAGE and transferred to PVDF membranes (Merck). Membranes were blocked with 0.1% casein/gelatin in Tris-buffered saline with Tween-20. Primary and secondary antibodies (Table S2) were reacted with in each blocking buffer. Signals were detected with a chemiluminescent reagent, ImmunoStar LD (Wako Pure Chemical Industries, Ltd., Osaka, Japan) or Western Lightning Plus ECL (PerkinElmer, Waltham, MA, USA). Signals were observed and band intensity was measured with a Fusion-Solo system (M&S Instruments, Tokyo, Japan). Full blot images for images in the figures are shown in Fig. S5.

Cell fractionation

Cell fractionation was performed with a cell fractionation kit (Abcam, Cambridge, UK) according to the manufacturer's instructions. Briefly, cells were resuspended in buffer A and permeabilized with detergent I. The cell suspension was then centrifuged at 10,000 ***g*** for 2 min. The resulting supernatant was collected as the cytosol fraction. The cytosol-depleted pellet was resuspended in buffer A and solubilized with detergent II. Following centrifugation at 10,000 ***g*** for 2 min, the supernatant was collected as the mitochondria-enriched fraction. The cytosol- and mitochondria-depleted pellet was resuspended in buffer A, and used as the nuclear fraction.

Immunoprecipitation

For immunoprecipitation, cells transfected with indicated plasmids were lysed with NP40 buffer (25 mM Tris-HCl pH 7.5, 150 mM NaCl, 1 mM EDTA, 1.0% NP40 and 5% glycerol) containing inhibitors (1 mM phenylmethylsulphonyl fluoride, 10 µg/ml aprotinin, 1 µg/ml leupeptin, 1 µg/ml pepstatin A, 1 mM Na_3VO_4 and 10 mM NaF) on ice for 20 min, after which the lysates were centrifuged at 20,000 ***g*** for 20 min at 4°C. The supernatants were collected and Flag M2 affinity beads (Sigma-Aldrich) were added and incubated at 4°C for 90 min. The beads were collected by centrifugation at 2500 ***g*** for 1 min and washed and boiled with 2× SDS sample buffer at 95°C for 5 min.

Cell cycle analysis

Cells were fixed with 70% ethanol and stored at −20°C for no longer than 24 h. Residual ethanol was eliminated from the cells being centrifuged (300 ***g*** for 3 min) and washed twice with fluorescence-activated cell sorter (FACS) buffer (2% fetal bovine serum and 1 mM EDTA in phosphate-buffered saline). For cell cycle analysis of the G0/1 to S phases, cells were re-stimulated with a medium containing 600 ng/ml nocodazole (Tocris Bioscience, Bristol, UK) to arrest dividing cells in metaphase. Cells were stained with 2 µl/ml Hoechst 33342 (AdipoGen Life Sciences, San Diego, CA, USA) and incubated for 20 min at room temperature. Stained cells were analyzed with a MACSQuant analyzer (Miltenyi Biotec, Tokyo, Japan). Data were analyzed with the software application FlowJo (Tomy Digital Biology, Tokyo, Japan).

Senescence β-galactosidase staining and FACS

Immunocytostaining for senescence β-galactosidase (SA-β-gal) was performed with a Senescence β-Galactosidase Staining Kit (Cell Signaling Technology, Danvers, MA, USA) according to the manufacturer's introductions. To induce cellular senescence, cells were serum-starved for 72 h and then fixated with a fixative solution for 15 min. Cells were washed twice in HEPES buffer and incubated with β-gal staining solution at 37°C overnight in a dry incubator. Signals were observed under a BZ-X800 microscope (Keyence). To conduct FACS of β-gal-labeled cells, cells were fixed with 4% formaldehyde at room temperature for 10 min. Senescence detection was performed with the Cell Event™ Senescence Green Detection Kit (Invitrogen, Waltham, MA, USA) according to the manufacturer's introductions. Stained cells were analyzed with a MACSQuant analyzer (Miltenyi Biotec), and data were analyzed with FlowJo (Tomy Digital Biology).

Real-time PCR

Isolation of total RNAs was performed with the RNeasy Mini Kit (Qiagen, Germantown, MD, USA). Reverse transcripts were obtained with PrimeScript Reverse Transcriptase (Takara Bio Inc.) and subjected to quantitative PCR (qPCR) with the PikoReal 96 system (Thermo Fisher Scientific). Reactions were performed in KAPA SYBR FAST qPCR Master Mix (Nippon Genetics, Tokyo, Japan) that included 0.2 µM of a specific primer set for each gene (Table S1). Data were calculated with the comparative CT method (ΔCT method) to estimate the mRNA copy number relative to that of *HPRT1* as an internal standard. The DNA sequence of the PCR product was confirmed with nucleotide sequencing (data not shown).

Statistical analysis

Each experiment was confirmed by at least three independent technical replicates per condition. Data are presented as the means±s.e.m. The Prism 7 software program (GraphPad, San Diego, CA, USA) was used for statistical analyses. Means between groups were compared with a paired two-tailed Student's *t*-test. Multiple intergroup differences were analyzed with one-way ANOVA followed by Tukey's multiple comparison test.

Acknowledgements

We would like to thank Dr. Yohei Katoh and Dr. Kazuhisa Nakayama at Kyoto University for technical supports to establish knockout cell lines by the CRISPR-Cas9 system. We also would like to thank Naoko Tago for technical supports of FACS analysis and Prof. Masao Okazaki for English proofreading.

Competing interests

The authors declare no competing or financial interests.

Author contributions

Conceptualization: A.K., S.Y., K. Yoshida; Methodology: A.K., S.Y., K.A., Y.S., K. Yamada; Validation: A.K., S.Y.; Formal analysis: A.K., S.Y.; Investigation: A.K., S.Y.; Resources: S.Y., Y.S., K. Yamada; Data curation: A.K., S.Y., K.A.; Writing - original draft: A.K., S.Y.; Writing - review & editing: A.K., S.Y., K. Yoshida; Visualization: A.K., S.Y.; Supervision: K. Yoshida; Project administration: S.Y., K. Yoshida; Funding acquisition: S.Y., K. Yoshida.

Funding

This work was partially supported by Japan Society for the Promotion of Science (JSPS) KAKENHI (grant numbers 21K06192 to S.Y. and 17H03584, 18K19484 and 20H03519 to K. Yoshida), the Jikei University Research Fund (to S.Y. and K. Yoshida), the Takeda Science Foundation (to S.Y.), and the Uehara Memorial Foundation (to S.Y. and K. Yoshida).

Peer review history
The peer review history is available online at https://journals.biologists.com/jcs/article-lookup/doi/10.1242/jcs.259514.

References

Abbas, T. and Dutta, A. (2009). p21 in cancer: intricate networks and multiple activities. *Nat. Rev. Cancer* **9**, 400-414. doi:10.1038/nrc2657
Ahn, J. Y., Schwarz, J. K., Piwnica-Worms, H. and Canman, C. E. (2000). Threonine 68 phosphorylation by ataxia telangiectasia mutated is required for efficient activation of Chk2 in response to ionizing radiation. *Cancer Res.* **60**, 5934-5936.
Ahn, J. Y., Li, X., Davis, H. L. and Canman, C. E. (2002). Phosphorylation of threonine 68 promotes oligomerization and autophosphorylation of the Chk2 protein kinase via the forkhead-associated domain. *J. Biol. Chem.* **277**, 19389-19395. doi:10.1074/jbc.M200822200
Aparicio, T., Baer, R. and Gautier, J. (2014). DNA double-strand break repair pathway choice and cancer. *DNA Repair* **19**, 169-175. doi:10.1016/j.dnarep.2014.03.014
Becker, W. and Sippl, W. (2011). Activation, regulation, and inhibition of DYRK1A. *FEBS J.* **278**, 246-256. doi:10.1111/j.1742-4658.2010.07956.x
Blackford, A. N. and Jackson, S. P. (2017). ATM, ATR, and DNA-PK: The Trinity at the Heart of the DNA Damage Response. *Mol. Cell* **66**, 801-817. doi:10.1016/j.molcel.2017.05.015
Branzei, D. and Foiani, M. (2008). Regulation of DNA repair throughout the cell cycle. *Nat. Rev. Mol. Cell Biol.* **9**, 297-308. doi:10.1038/nrm2351
Brown, J. S. and Jackson, S. P. (2015). Ubiquitylation, neddylation and the DNA damage response. *Open Biol.* **5**, 150018. doi:10.1098/rsob.150018
Brownell, J. E., Sintchak, M. D., Gavin, J. M., Liao, H., Bruzzese, F. J., Bump, N. J., Soucy, T. A., Milhollen, M. A., Yang, X., Burkhardt, A. L. et al. (2010). Substrate-assisted inhibition of ubiquitin-like protein-activating enzymes: the NEDD8 E1 inhibitor MLN4924 forms a NEDD8-AMP mimetic in situ. *Mol. Cell* **37**, 102-111. doi:10.1016/j.molcel.2009.12.024
Cech, T. R. (2004). Beginning to understand the end of the chromosome. *Cell* **116**, 273-279. doi:10.1016/s0092-8674(04)00038-8
Childs, B. G., Baker, D. J., Kirkland, J. L., Campisi, J. and van Deursen, J. M. (2014). Senescence and apoptosis: dueling or complementary cell fates? *EMBO Rep.* **15**, 1139-1153. doi:10.15252/embr.201439245
Ciccia, A. and Elledge, S. J. (2010). The DNA damage response: making it safe to play with knives. *Mol. Cell* **40**, 179-204. doi:10.1016/j.molcel.2010.09.019
Coates, P. J., Lorimore, S. A. and Wright, E. G. (2005). Cell and tissue responses to genotoxic stress. *J. Pathol.* **205**, 221-235. doi:10.1002/path.1701
Coppé, J. P., Patil, C. K., Rodier, F., Sun, Y., Muñoz, D. P., Goldstein, J., Nelson, P. S., Desprez, P. Y. and Campisi, J. (2008). Senescence-associated secretory phenotypes reveal cell-nonautonomous functions of oncogenic RAS and the p53 tumor suppressor. *PLoS Biol.* **6**, e301. doi:10.1371/journal.pbio.0060301
Deman, J. and Van Larebeke, N. (2001). Carcinogenesis: mutations and mutagens. *Tumour Biol.* **22**, 191-202. doi:10.1159/000050615
Drainas, A. P., Lambuta, R. A., Ivanova, I., Serçin, Ö., Sarropoulos, I., Smith, M. L., Efthymiopoulos, T., Raeder, B., Stütz, A. M. , Waszak, S. M. et al. (2020). Genome-wide screens implicate loss of cullin ring ligase 3 in persistent proliferation and genome instability in TP53-deficient cells. *Cell Rep.* **31**, 107465. doi:10.1016/j.celrep.2020.03.029
Enomoto, Y., Yamashita, S., Yoshinaga, Y., Fukami, Y., Miyahara, S., Nabeshima, K. and Iwasaki, A. (2014). Downregulation of DYRK2 can be a predictor of recurrence in early stage breast cancer. *Tumour Biol.* **35**, 11021-11025. doi:10.1007/s13277-014-2413-z
Hafner, A., Bulyk, M. L., Jambhekar, A. and Lahav, G. (2019). The multiple mechanisms that regulate p53 activity and cell fate. *Nat. Rev. Mol. Cell Biol.* **20**, 199-210. doi:10.1038/s41580-019-0110-x
Ito, D., Yogosawa, S., Mimoto, R., Hirooka, S., Horiuchi, T., Eto, K., Yanaga, K. and Yoshida, K. (2017). Dual-specificity tyrosine-regulated kinase 2 is a suppressor and potential prognostic marker for liver metastasis of colorectal cancer. *Cancer Sci.* **108**, 1565-1573. doi:10.1111/cas.13280
Jackson, S. P. and Bartek, J. (2009). The DNA-damage response in human biology and disease. *Nature* **461**, 1071-1078. doi:10.1038/nature08467
Jia, L., Li, H. and Sun, Y. (2011). Induction of p21-dependent senescence by an NAE inhibitor, MLN4924, as a mechanism of growth suppression. *Neoplasia* **13**, 561-569. doi:10.1593/neo.11420
Jiang, Y. and Jia, L. (2015). Neddylation pathway as a novel anti-cancer target: mechanistic investigation and therapeutic implication. *Anticancer Agents Med. Chem.* **15**, 1127-1133. doi:10.2174/1871520615666150305111257
Jung, H. Y., Wang, X., Jun, S. and Park, J. I. (2013). Dyrk2-associated EDD-DDB1-VprBP E3 ligase inhibits telomerase by TERT degradation. *J. Biol. Chem.* **288**, 7252-7262. doi:10.1074/jbc.M112.416792
Katoh, Y., Michisaka, S., Nozaki, S., Funabashi, T., Hirano, T., Takei, R. and Nakayama, K. (2017). Practical method for targeted disruption of cilia-related genes by using CRISPR/Cas9-mediated, homology-independent knock-in system. *Mol. Biol. Cell* **28**, 898-906. doi:10.1091/mbc.E17-01-0051
Kinzler, K. W. and Vogelstein, B. (1997). Cancer-susceptibility genes. Gatekeepers and caretakers. *Nature* **386**, 761-763. doi:10.1038/386761a0
Kumamoto, T., Yamada, K., Yoshida, S., Aoki, K., Hirooka, S., Eto, K., Yanaga, K. and Yoshida, K. (2020). Impairment of DYRK2 by DNMT1–mediated transcription augments carcinogenesis in human colorectal cancer. *Int. J. Oncol.* **56**, 1529-1539. doi:10.3892/ijo.2020.5020
Loeb, L. A. (1994). Microsatellite instability: marker of a mutator phenotype in cancer. *Cancer Res.* **54**, 5059-5063.
Ma, T., Chen, Y., Zhang, F., Yang, C.-Y., Wang, S. and Yu, X. (2013). RNF111-dependent neddylation activates DNA damage-induced ubiquitination. *Mol. Cell* **49**, 897-907. doi:10.1016/j.molcel.2013.01.006
McKinnon, P. J. (2017). Genome integrity and disease prevention in the nervous system. *Genes Dev.* **31**, 1180-1194. doi:10.1101/gad.301325.117
Milhollen, M. A., Narayanan, U., Soucy, T. A., Veiby, P. O., Smith, P. G. and Amidon, B. (2011). Inhibition of NEDD8-activating enzyme induces rereplication and apoptosis in human tumor cells consistent with deregulating CDT1 turnover. *Cancer Res.* **71**, 3042-3051. doi:10.1158/0008-5472.Can-10-2122
Mimoto, R., Taira, N., Takahashi, H., Yamaguchi, T., Okabe, M., Uchida, K., Miki, Y. and Yoshida, K. (2013). DYRK2 controls the epithelial-mesenchymal transition in breast cancer by degrading Snail. *Cancer Lett.* **339**, 214-225. doi:10.1016/j.canlet.2013.06.005
Mimoto, R., Nihira, N. T., Hirooka, S., Takeyama, H. and Yoshida, K. (2017). Diminished DYRK2 sensitizes hormone receptor-positive breast cancer to everolimus by the escape from degrading mTOR. *Cancer Lett.* **384**, 27-38. doi:10.1016/j.canlet.2016.10.015
Negrini, S., Gorgoulis, V. G. and Halazonetis, T. D. (2010). Genomic instability — an evolving hallmark of cancer. *Nat. Rev. Mol. Cell Biol.* **11**, 220-228. doi:10.1038/nrm2858
Petroski, M. D. and Deshaies, R. J. (2005). Function and regulation of cullin-RING ubiquitin ligases. *Nat. Rev. Mol. Cell Biol.* **6**, 9-20. doi:10.1038/nrm1547
Rogakou, E. P., Pilch, D. R., Orr, A. H., Ivanova, V. S. and Bonner, W. M. (1998). DNA double-stranded breaks induce histone H2AX phosphorylation on serine 139. *J. Biol. Chem.* **273**, 5858-5868. doi:10.1074/jbc.273.10.5858
Schwertman, P., Bekker-Jensen, S. and Mailand, N. (2016). Regulation of DNA double-strand break repair by ubiquitin and ubiquitin-like modifiers. *Nat. Rev. Mol. Cell Biol.* **17**, 379-394. doi:10.1038/nrm.2016.58
Shen, Y., Zhang, L., Wang, D., Bao, Y., Liu, C., Xu, Z., Huang, W. and Cheng, C. (2017). Regulation of Glioma Cells Migration by DYRK2. *Neurochem. Res.* **42**, 3093-3102. doi:10.1007/s11064-017-2345-2
Shieh, S.-Y., Ikeda, M., Taya, Y. and Prives, C. (1997). DNA damage-induced phosphorylation of p53 alleviates inhibition by MDM2. *Cell* **91**, 325-334. doi:10.1016/s0092-8674(00)80416-x
Shukla, M., Chinchalongporn, V. and Govitrapong, P. (2020). Melatonin prevents neddylation dysfunction in Aβ42-Exposed SH-SY5Y neuroblastoma cells by regulating the amyloid precursor protein- binding protein 1 pathway. *Curr. Alzheimer Res.* **17**, 446-459. doi:10.2174/1567205017666200624201356
Siliciano, J. D., Canman, C. E., Taya, Y., Sakaguchi, K., Appella, E. and Kastan, M. B. (1997). DNA damage induces phosphorylation of the amino terminus of p53. *Genes Dev.* **11**, 3471-3481. doi:10.1101/gad.11.24.3471
Soucy, T. A., Smith, P. G. and Rolfe, M. (2009). Targeting NEDD8-activated cullin-RING ligases for the treatment of cancer. *Clin. Cancer Res.* **15**, 3912-3916. doi:10.1158/1078-0432.Ccr-09-0343
Taira, N., Nihira, K., Yamaguchi, T., Miki, Y. and Yoshida, K. (2007). DYRK2 is targeted to the nucleus and controls p53 via Ser46 phosphorylation in the apoptotic response to DNA damage. *Mol. Cell* **25**, 725-738. doi:10.1016/j.molcel.2007.02.007
Taira, N., Yamamoto, H., Yamaguchi, T., Miki, Y. and Yoshida, K. (2010). ATM augments nuclear stabilization of DYRK2 by inhibiting MDM2 in the apoptotic response to DNA damage. *J. Biol. Chem.* **285**, 4909-4919. doi:10.1074/jbc.M109.042341
Taira, N., Mimoto, R., Kurata, M., Yamaguchi, T., Kitagawa, M., Miki, Y. and Yoshida, K. (2012). DYRK2 priming phosphorylation of c-Jun and c-Myc modulates cell cycle progression in human cancer cells. *J. Clin. Invest.* **122**, 859-872. doi:10.1172/jci60818
Takahashi, A., Okada, R., Nagao, K., Kawamata, Y., Hanyu, A., Yoshimoto, S., Takasugi, M., Watanabe, S., Kanemaki, M. T., Obuse, C. et al. (2017). Exosomes maintain cellular homeostasis by excreting harmful DNA from cells. *Nat. Commun.* **8**, 15287. doi:10.1038/ncomms15287
Takahashi, A., Loo, T. M., Okada, R., Kamachi, F., Watanabe, Y., Wakita, M., Watanabe, S., Kawamoto, S., Miyata, K., Barber, G. N. et al. (2018). Downregulation of cytoplasmic DNases is implicated in cytoplasmic DNA accumulation and SASP in senescent cells. *Nat. Commun.* **9**, 1249. doi:10.1038/s41467-018-03555-8
Walsh, C. T., Garneau-Tsodikova, S. and Gatto, G. J.Jr. (2005). Protein posttranslational modifications: the chemistry of proteome diversifications. *Angew. Chem. Int. Ed. Engl.* **44**, 7342-7372. doi:10.1002/anie.200501023
Wang, J. and Lindahl, T. (2016). Maintenance of genome stability. *Genomics Proteomics Bioinformatics* **14**, 119-121. doi:10.1016/j.gpb.2016.06.001

Wang, Z., Zhu, W.-G. and Xu, X. (2017). Ubiquitin-like modifications in the DNA damage response. *Mutat. Res.* **803-805**, 56-75. doi:10.1016/j.mrfmmm.2017.07.001

Watson, I. R., Irwin, M. S. and Ohh, M. (2011). NEDD8 pathways in cancer, Sine Quibus Non. *Cancer Cell* **19**, 168-176. doi:10.1016/j.ccr.2011.01.002

Yamamoto, T., Taira Nihira, N., Yogosawa, S., Aoki, K., Takeda, H., Sawasaki, T. and Yoshida, K. (2017). Interaction between RNF8 and DYRK2 is required for the recruitment of DNA repair molecules to DNA double-strand breaks. *FEBS Lett.* **591**, 842-853. doi:10.1002/1873-3468.12596

Yamashita, S., Chujo, M., Moroga, T., Anami, K., Tokuishi, K., Miyawaki, M., Kawano, Y., Takeno, S., Yamamoto, S. and Kawahara, K. (2009a). DYRK2 expression may be a predictive marker for chemotherapy in non-small cell lung cancer. *Anticancer Res.* **29**, 2753-2757.

Yamashita, S., Chujo, M., Tokuishi, K., Anami, K., Miyawaki, M., Yamamoto, S. and Kawahara, K. (2009b). Expression of dual-specificity tyrosine-(Y)-phosphorylation-regulated kinase 2 (DYRK2) can be a favorable prognostic marker in pulmonary adenocarcinoma. *J. Thorac. Cardiovasc. Surg.* **138**, 1303-1308. doi:10.1016/j.jtcvs.2009.08.003

Yee, A. S., Paulson, E. K., McDevitt, M. A., Rieger-Christ, K., Summerhayes, I., Berasi, S. P., Kim, J., Huang, C. Y. and Zhang, X. (2004). The HBP1 transcriptional repressor and the p38 MAP kinase: unlikely partners in G1 regulation and tumor suppression. *Gene* **336**, 1-13. doi:10.1016/j.gene.2004.04.004

Yokoyama-Mashima, S., Yogosawa, S., Kanegae, Y., Hirooka, S., Yoshida, S., Horiuchi, T., Ohashi, T., Yanaga, K., Saruta, M., Oikawa, T. et al. (2019). Forced expression of DYRK2 exerts anti-tumor effects via apoptotic induction in liver cancer. *Cancer Lett.* **451**, 100-109. doi:10.1016/j.canlet.2019.02.046

Yoshida, S. and Yoshida, K. (2019). Multiple functions of DYRK2 in cancer and tissue development. *FEBS Lett.* **593**, 2953-2965. doi:10.1002/1873-3468.13601

Yoshida, S., Aoki, K., Fujiwara, K., Nakakura, T., Kawamura, A., Yamada, K., Ono, M., Yogosawa, S. and Yoshida, K. (2020). The novel ciliogenesis regulator DYRK2 governs Hedgehog signaling during mouse embryogenesis. *eLife* **9**, e57381. doi:10.7554/eLife.57381

Zhang, X., Xu, P., Ni, W., Fan, H., Xu, J., Chen, Y., Huang, W., Lu, S., Liang, L., Liu, J. et al. (2016). Downregulated DYRK2 expression is associated with poor prognosis and Oxaliplatin resistance in hepatocellular carcinoma. *Pathol. Res. Pract.* **212**, 162-170. doi:10.1016/j.prp.2016.01.002

Zhang, Y., Guo, Q., Jiang, G. and Zhang, C. (2021). Dysfunction of Cullin 3 RING E3 ubiquitin ligase causes vasoconstriction and increased sodium reabsorption in diabetes. *Arch. Biochem. Biophys.* **710**, 109000. doi:10.1016/j.abb.2021.109000

Fig. S1.

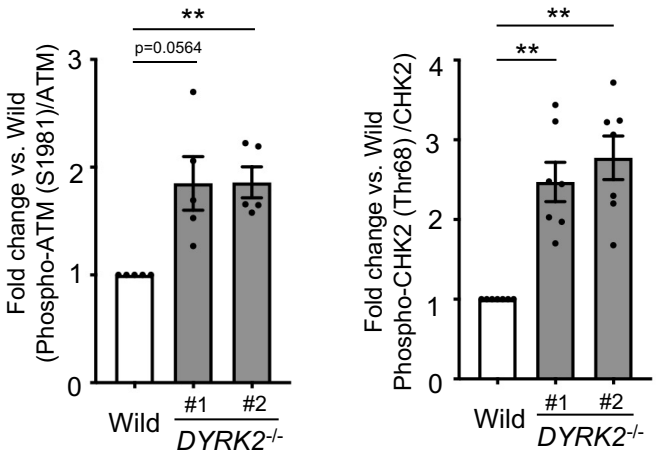

Fig. S1. (Related to Fig. 1). Quantification of phosphorylated ATM and CHK2

Protein level as fold changes of phospho-ATM and phospho-CHK2 in (Fig. 1E) was calculated by comparing protein levels relative to those of wild-type hTERT-RPE1 cells in after normalization to the total ATM and CHK2, respectively. Data are presented as the means ± SEM (n = 5 and 7 technical replicates per condition, respectively). The statistical significance was determined by one-way ANOVA followed by Tukey's multiple comparison test. (**) $P<0.01$.

Fig. S2.

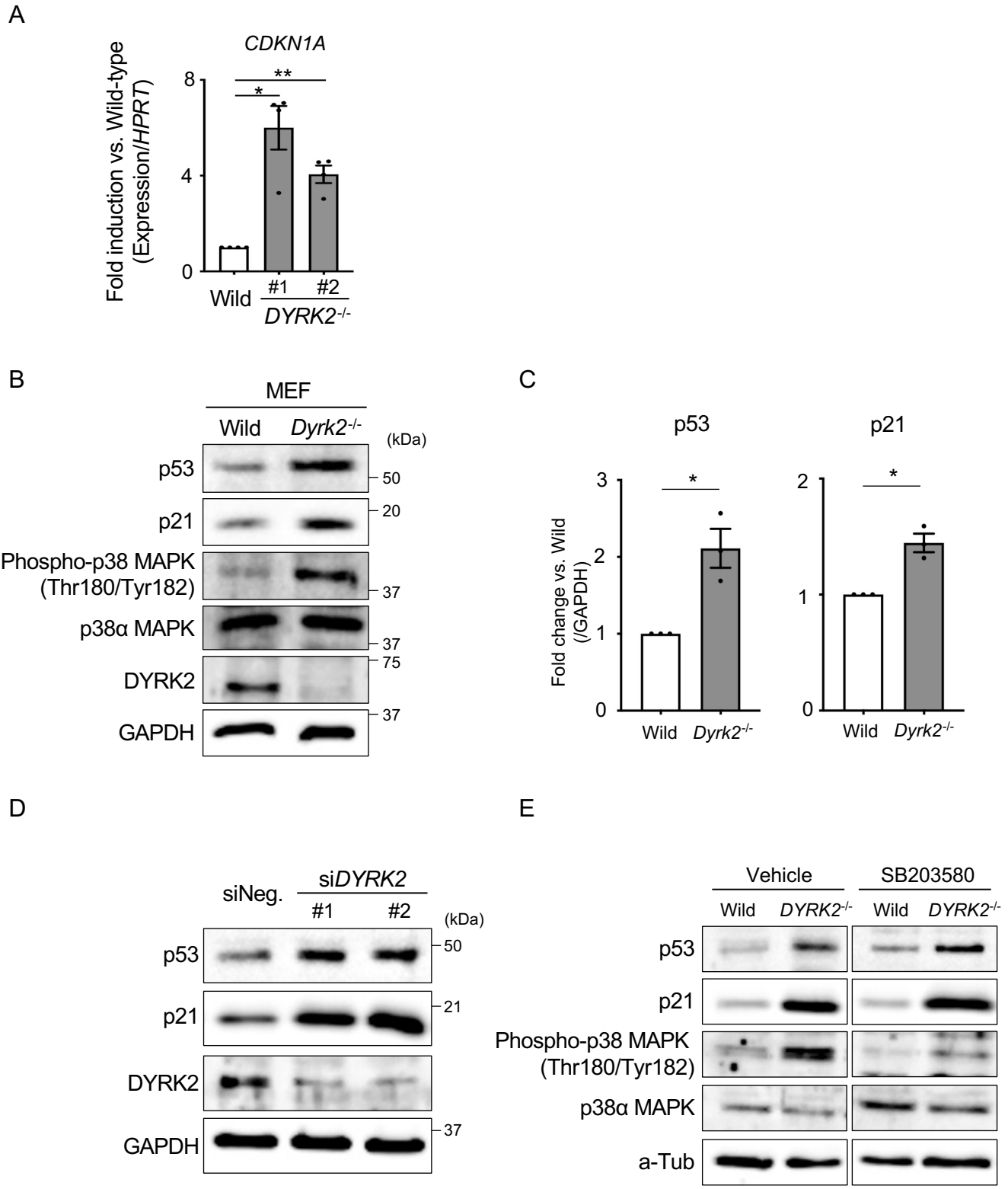

Fig. S2. (Related to Fig. 3). DYRK2 depletion cause p21 and p38 MAPK activation via p53

(A) Expression of the *CDKN1A* in wild-type and *DYRK2*$^{-/-}$ hTERT-RPE1 cells was measured by qPCR. *HPRT1* was used as an internal standard, and fold change was calculated by comparing expression levels relative to those of wild-type. Data are presented as the means ± SEM (n = 4 technical replicates per condition). The statistical significance was determined by one-way ANOVA followed by Tukey's multiple comparison test. (*) $P<0.05$, (**) $P<0.01$. (B & C) Protein levels of p53, p21, phospho-p38 MAPK, p38a MAPK, and DYRK2 in wild-type and *Dyrk2*$^{-/-}$ MEFs were measured by immuno-blotting. Protein level as fold changes of p53 and p21 w~as calculated by comparing protein levels relative to those of wild-type MEFs in after normalization to the GAPDH loading control (C). Data are presented as the means ± SEM (n = 3 biological replicates per condition). The statistical significance between wild-type and *Dyrk2*$^{-/-}$ was determined by the Student's t-test. (*) $P<0.05$. (D) Protein levels of p53, p21, phospho-p38 MAPK, p38a MAPK, and DYRK2 in hTERT-RPE1 cells treated with siNegative or two independent si*DYRK2* were measured by immuno-blotting. GAPDH serves as a loading control. (E) Protein levels of p53, p21, phospho-p38 MAPK, and p38a MAPK in wild-type and *DYRK2*$^{-/-}$ hTERT-RPE1 cells treated with SB203580 (a p38 MAPK inhibitor) were measured by immuno-blotting. aTubulin serves as a loading control.

Fig. S3.

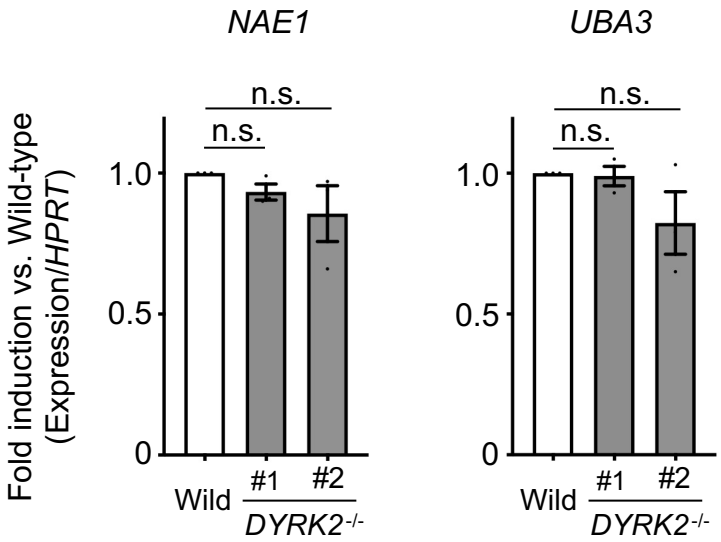

Fig. S3. (Related to Fig. 4). Expression of the *NAE1* and *UBA3*

Expression of the *NAE1* and *UBA3* in wild-type and *DYRK2*$^{-/-}$ hTERT-RPE1 cells was measured by qPCR. *HPRT1* was used as an internal standard, and fold change was calculated by comparing expression levels relative to those of wild-type. Data are presented as the means ± SEM (n = 3 technical replicates per condition). The statistical significance was determined by one-way ANOVA followed by Tukey's multiple comparison test.

Fig. S4.

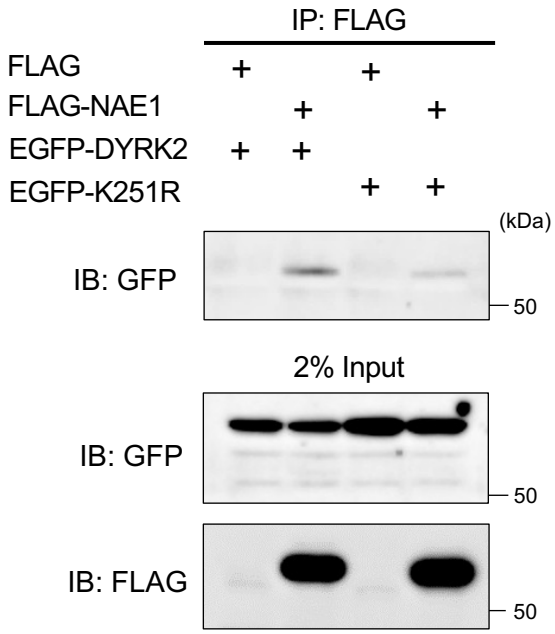

Fig. S4. (Related to Fig. 4). DYRK2-K251R also interacts with NAE1

Lysates from Lenti-X 293T cells co-transfected with an empty vector (pcDNA3-FLAG), and FLAG-NAE1 with EGFP-DYRK2, or EGFP-DYRK2-K251R were immunoprecipitated with anti-Flag agarose. Immunoprecipitates and input were then subjected to immune-blot analysis with anti-GFP or anti-FLAG.

Fig. S5. (Blot Transparency)

Fig. 1.

E

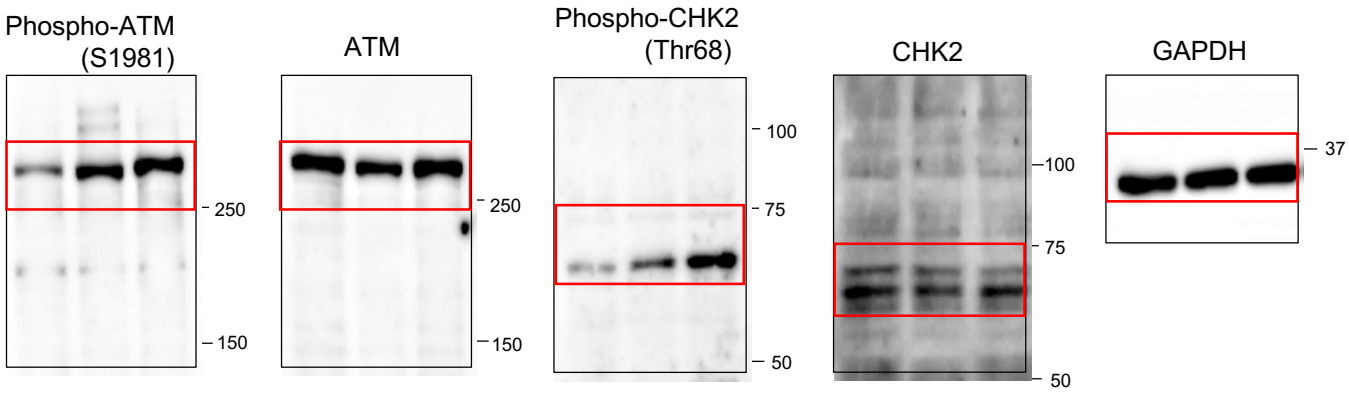

Fig. 2.

D

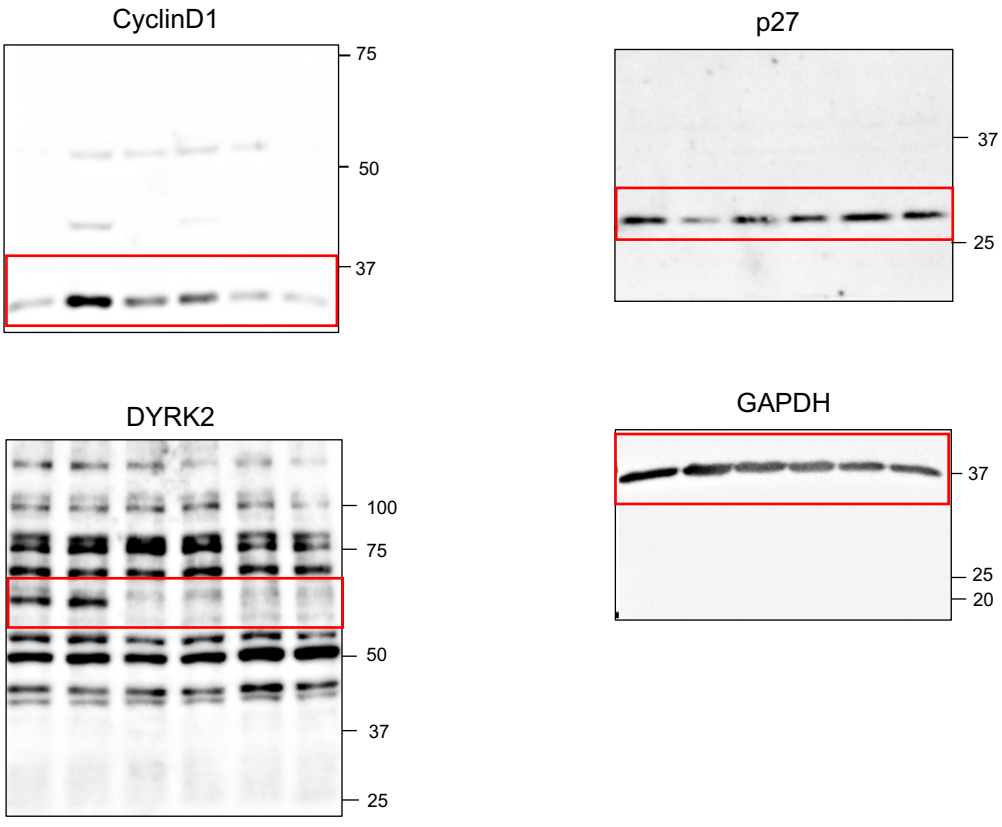

Fig. 3.

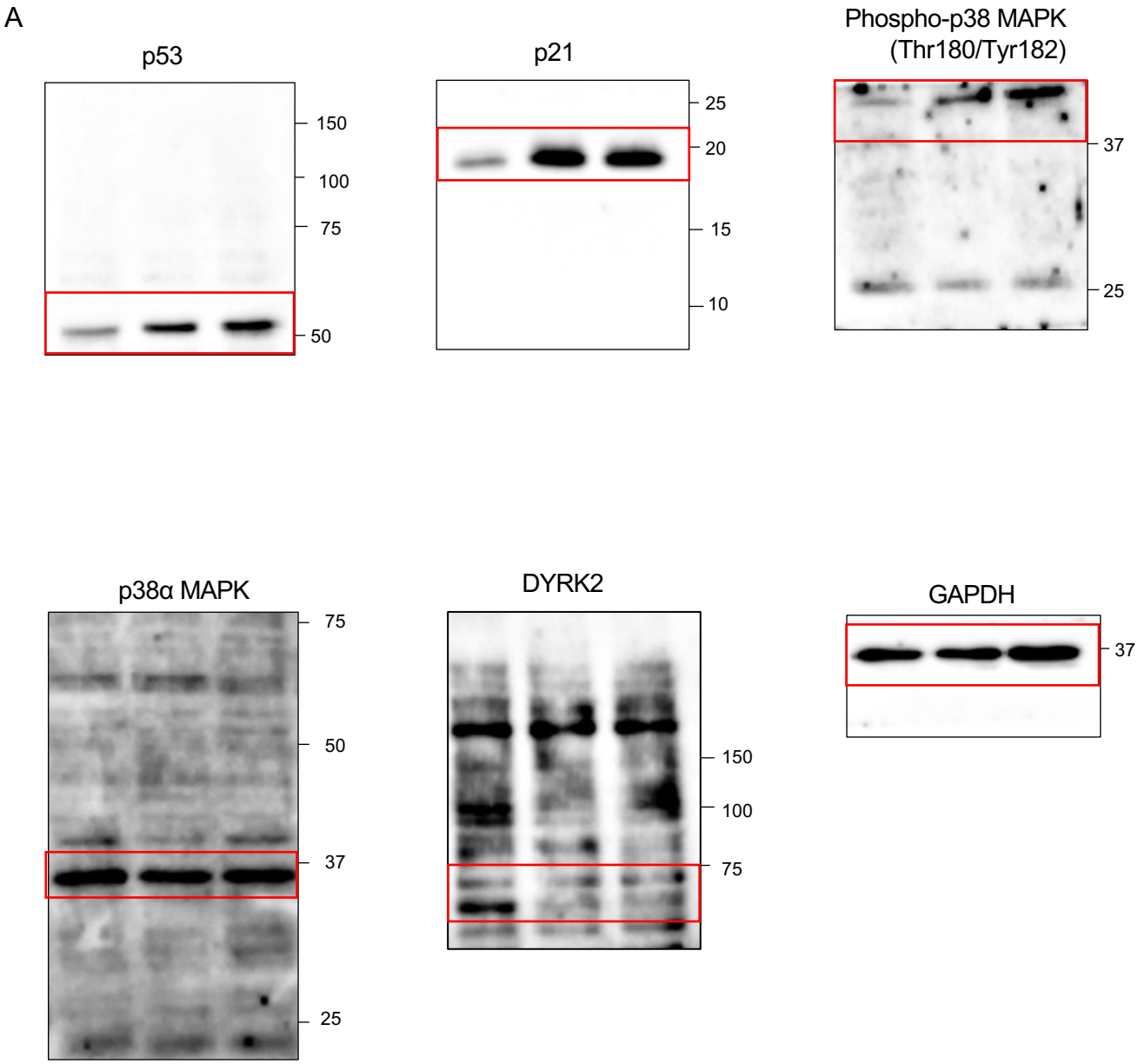

Fig. 3.

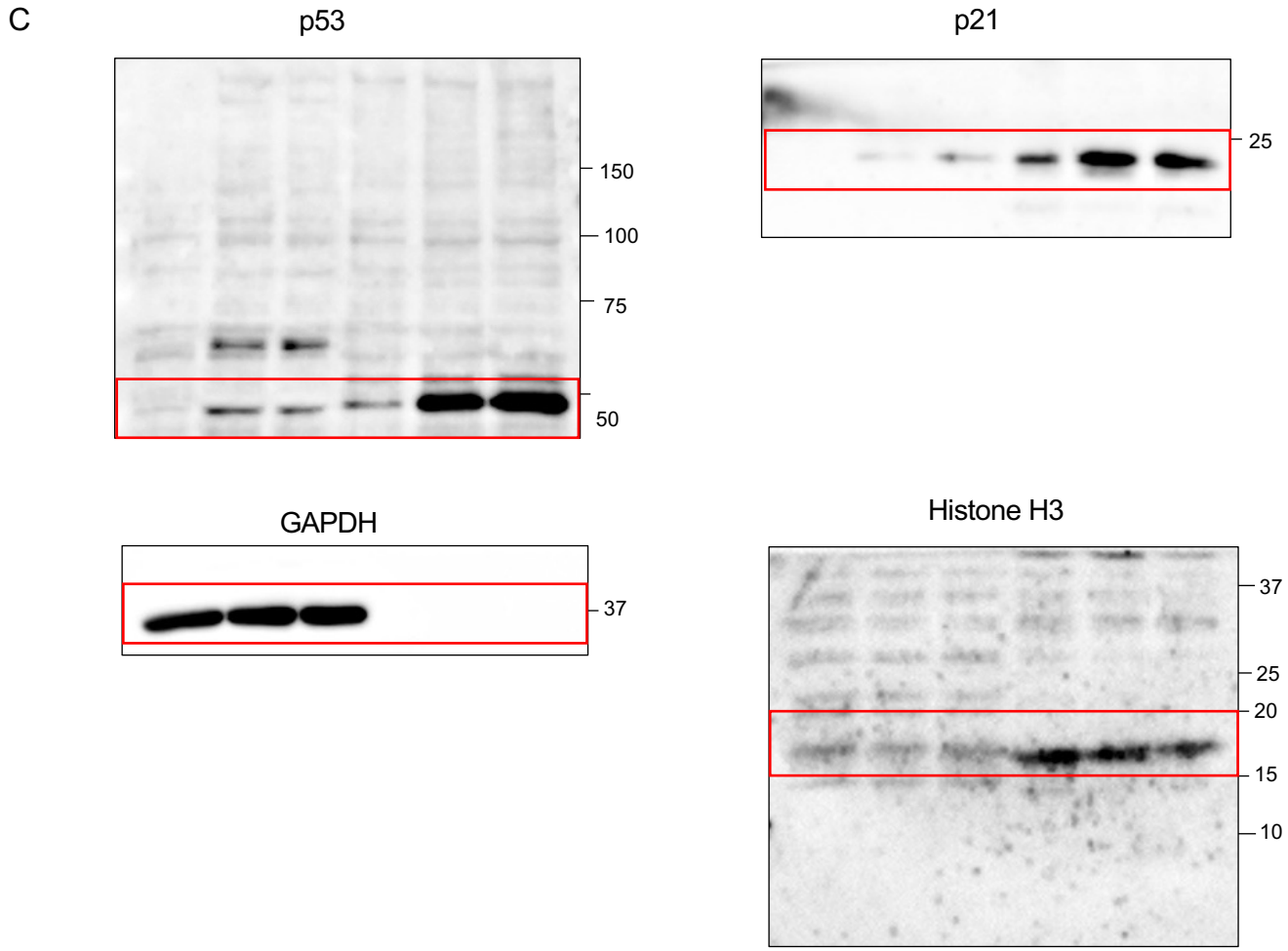

Fig. 3.

E

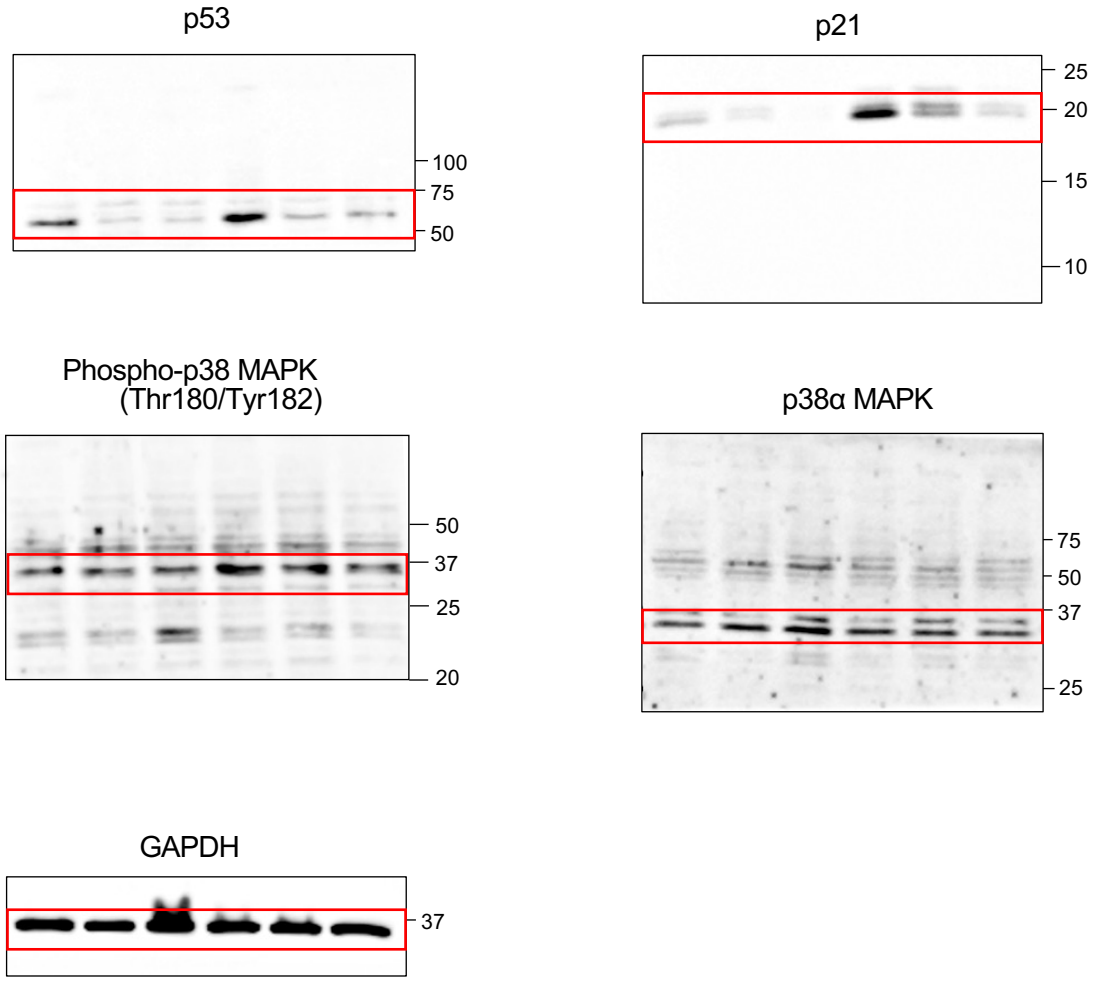

Fig. 4.

A

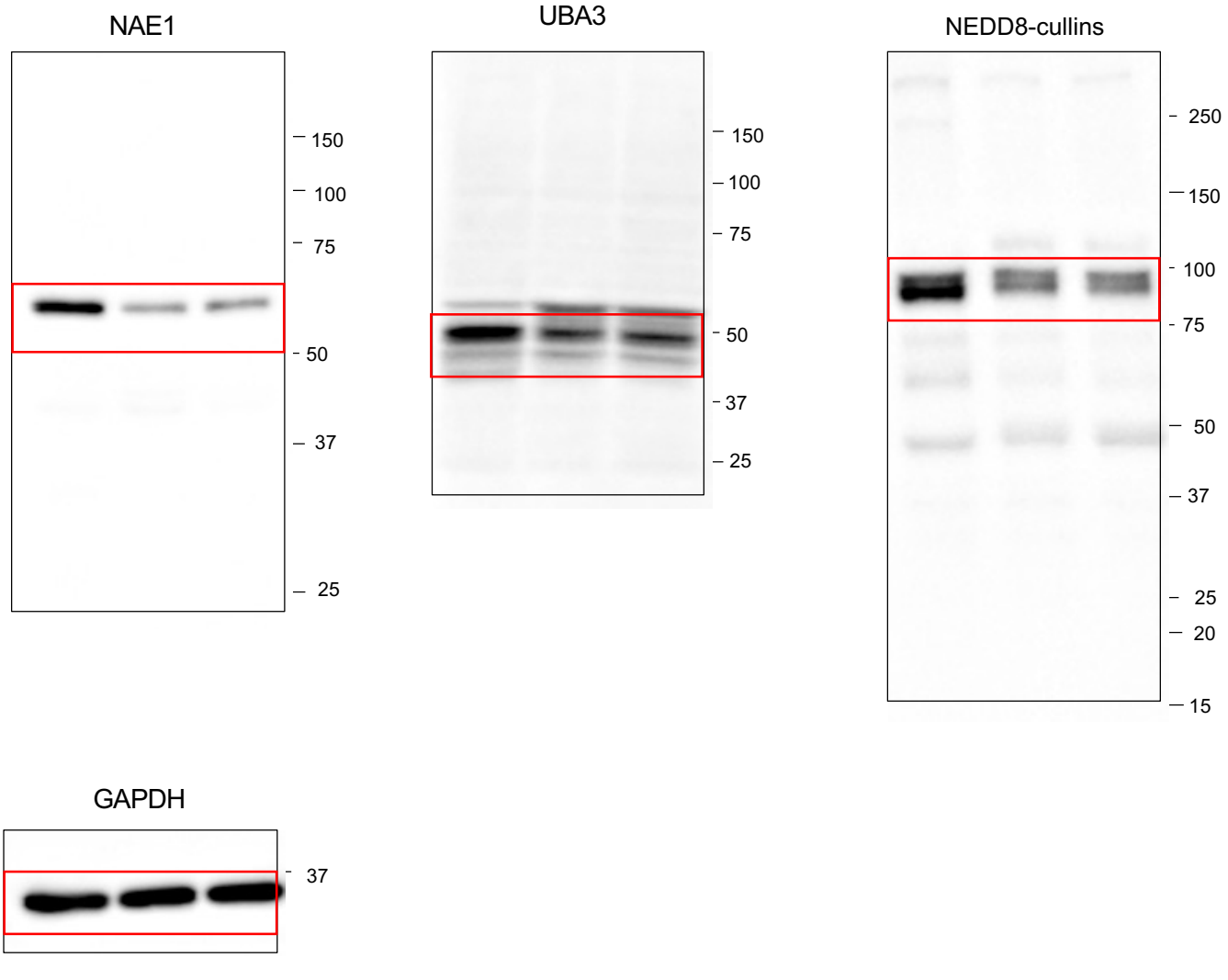

Fig. 4.

B

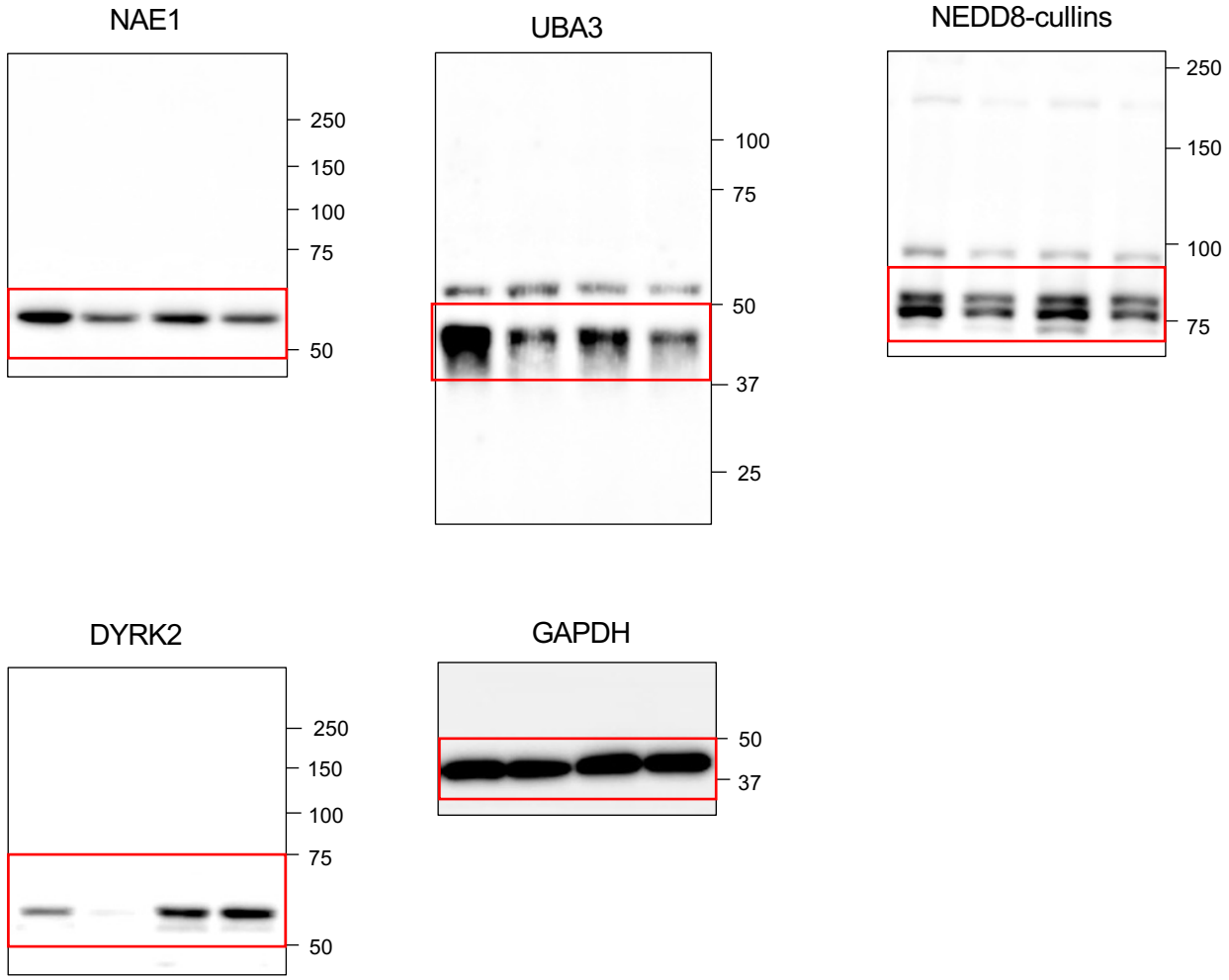

Fig. 4.

C

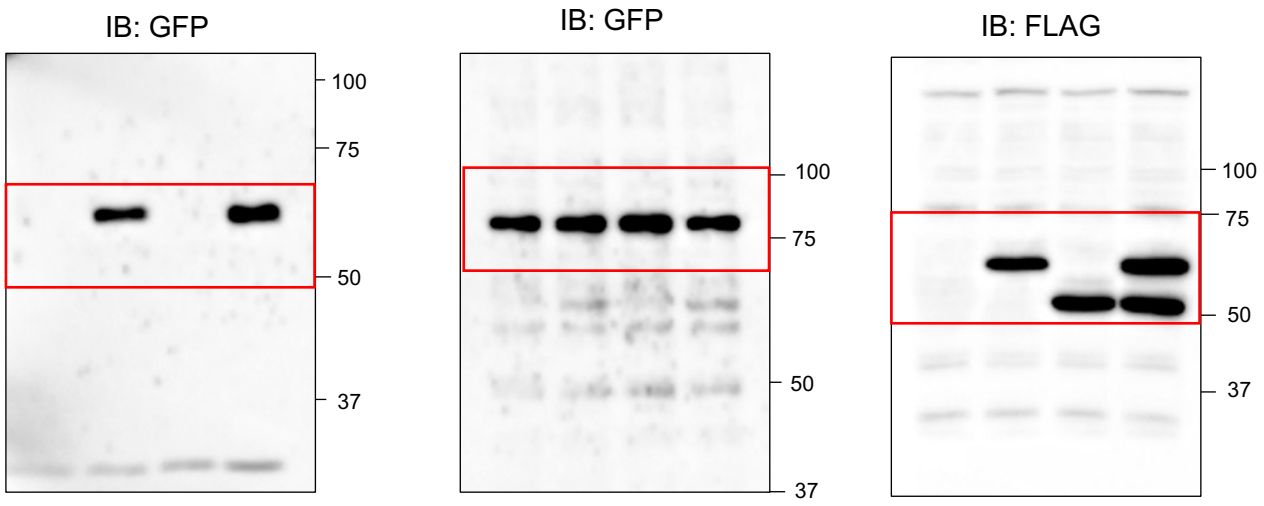

D

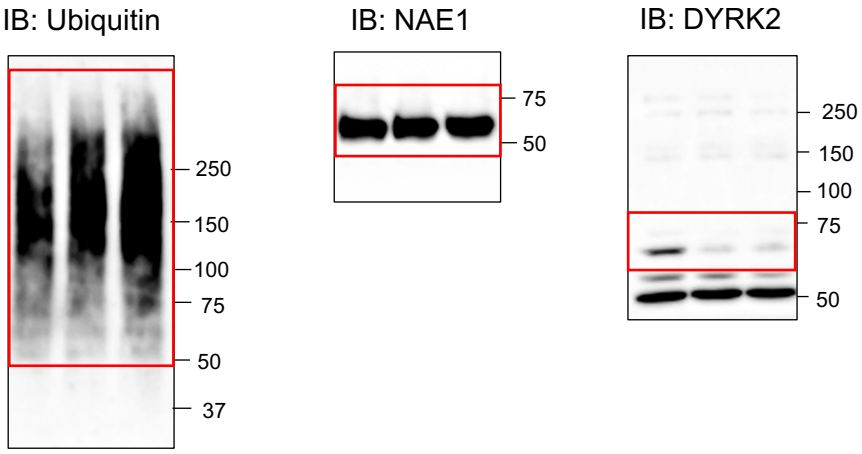

Fig. S2.

B

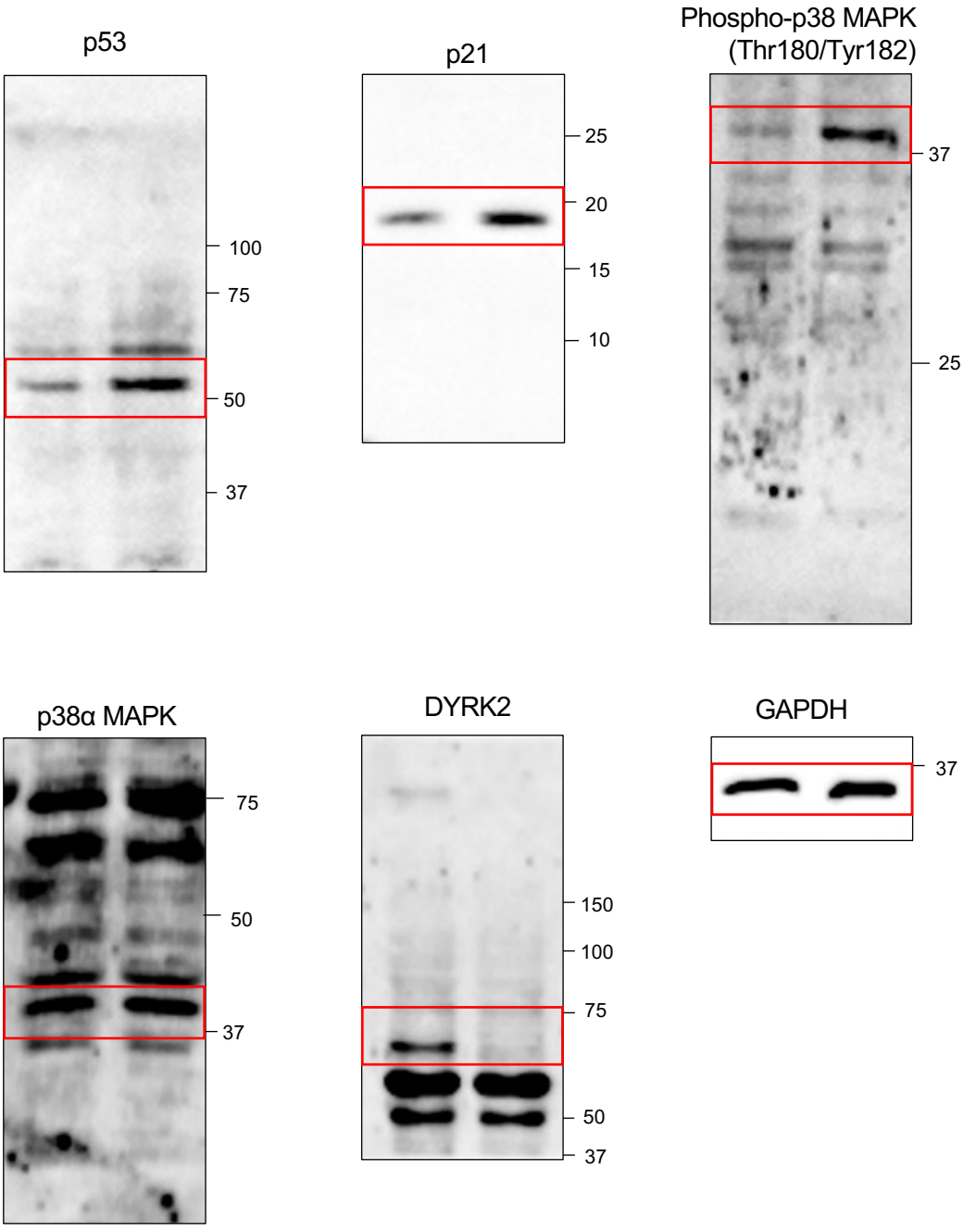

Fig. S2.

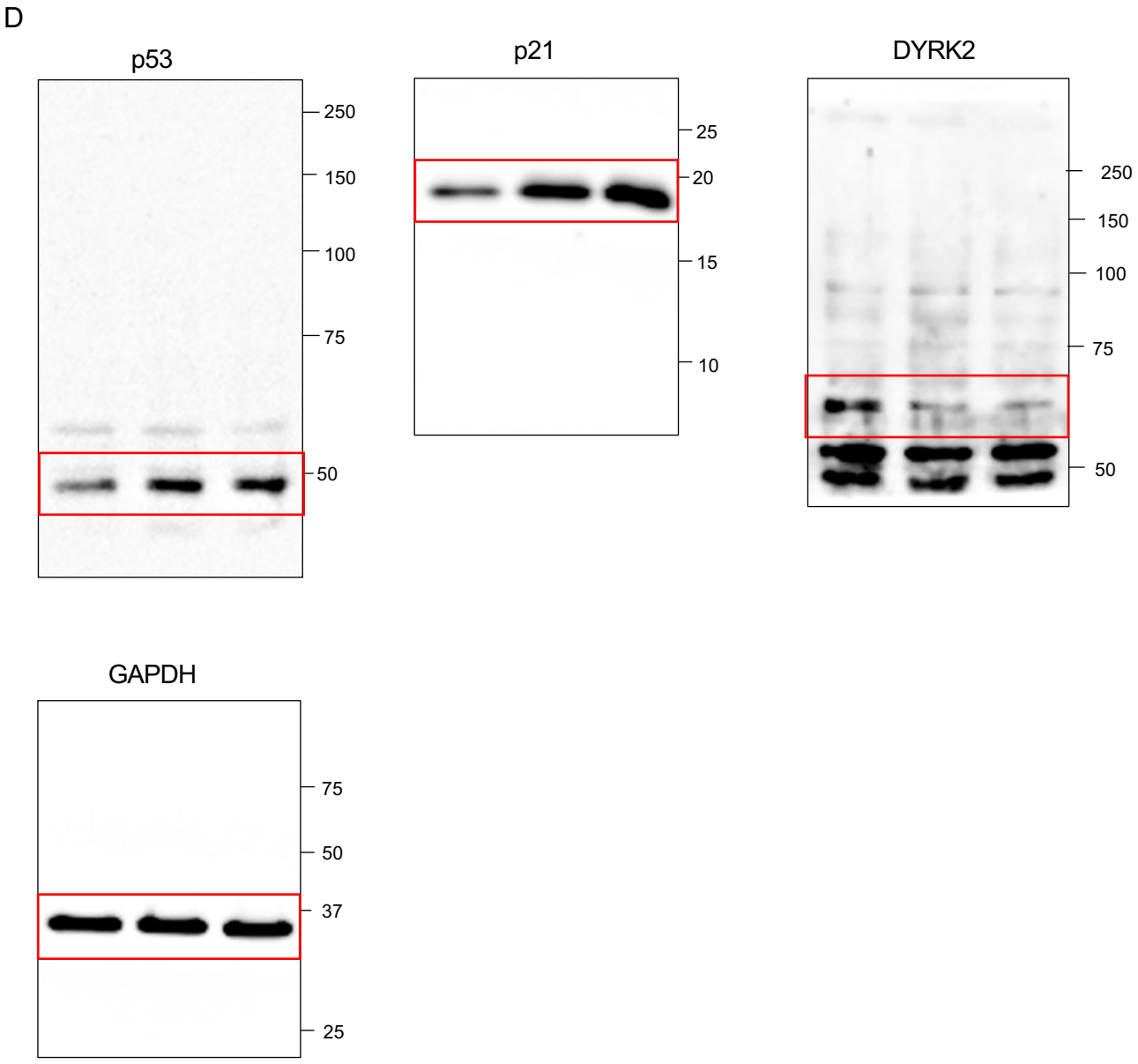

Fig. S2.

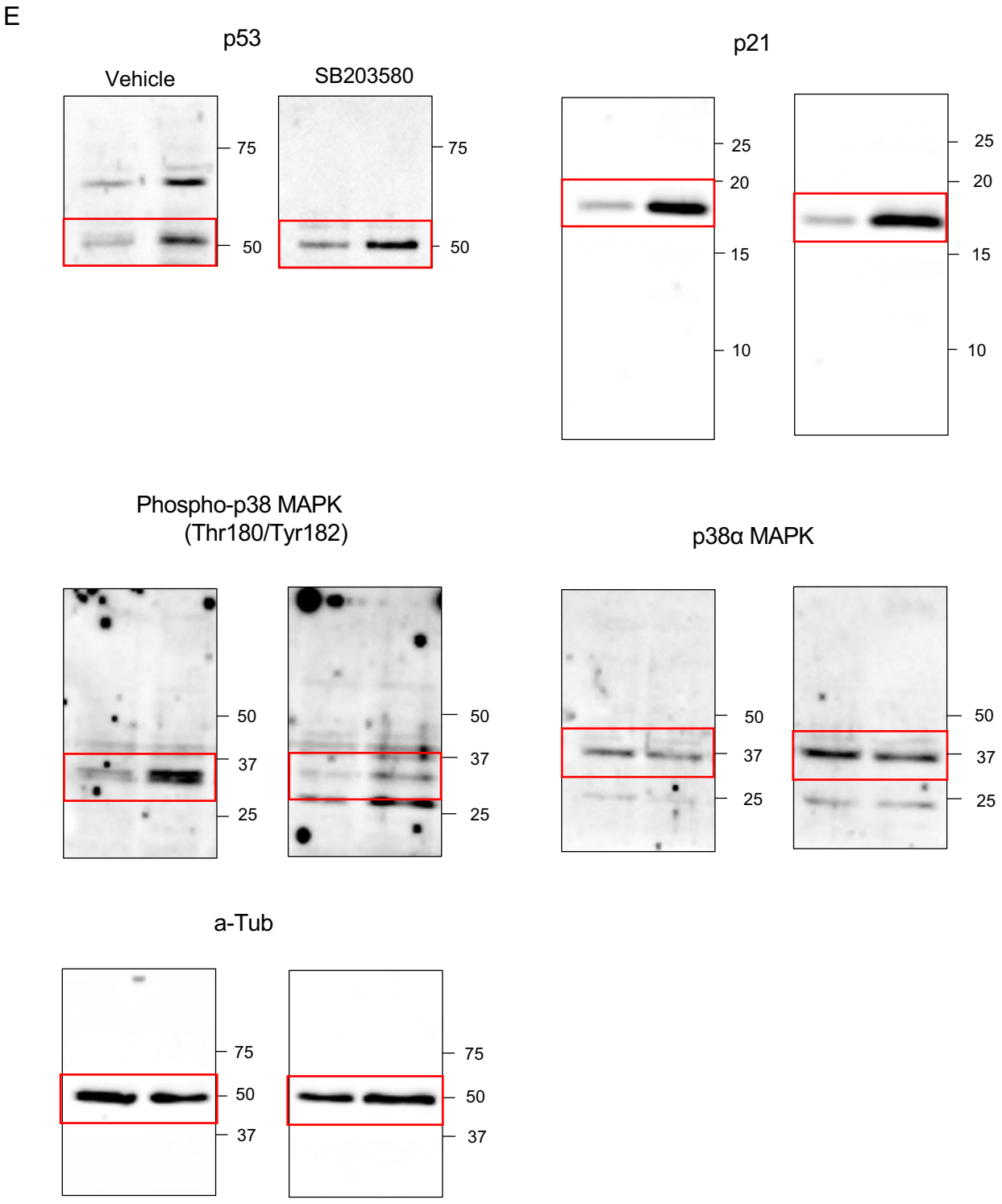

Fig. S4.

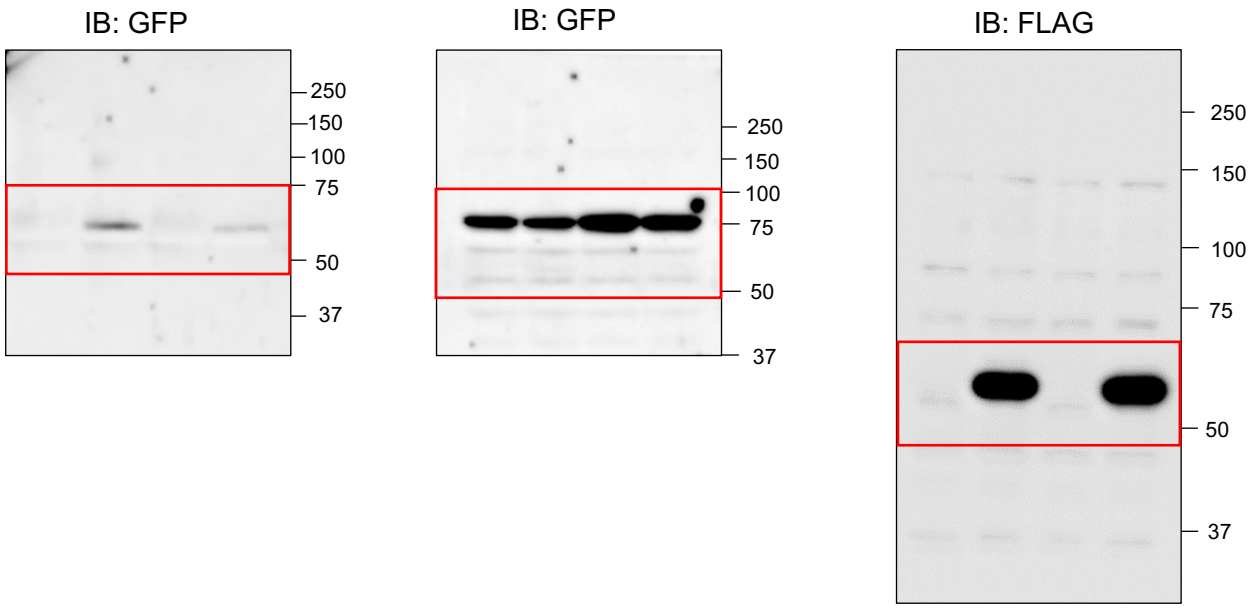

Table S1. List of primer sets

For cloning			
Gene	Sequence (5'→3')		Accession number
human *DYRK2 CDS*	Forward	GGACTCAGATCTCGAGACAATGATCACCTGCATGTCG	NM_003583.4
	Reverse	GTCGACTGCAGAATTCTCAGCTAACAAGTTTTGGCA	
human *NAE1 CDS*	Forward	CGATGACAAGGGATCCGCGCAGCTGGGAAAGCTG	NM_003905.4
	Reverse	GATATCTGCAGAATTCCTACAACTGGAAAGTTGCTG	
human *UBA3 CDS*	Forward	CGATGACAAGGGATCCGCGGATGGCGAGGAGCCG	NM_003968.4
	Reverse	GATATCTGCAGAATTCTTAAGAAGTAAAATGAAGTTTGA	
For real-time PCR			
Gene	Sequence (5'→3')		Accession number
human CDKN1A	Forward	TAGCAGCGGAACAAGGAG	NM_000389.4
	Reverse	AAACGGGAACCAGGACAC	
human *HPRT1*	Forward	GGACTAATTATGGACAGGACTG	NM_000194.3
	Reverse	GCTCTTCAGTCTGATAAAATCTAC	
human NAE1	Forward	GCTCAAGGAGCAGAAGTACGAC	NM_001018159.2
	Reverse	ATGAGCAGATTCTAAAGCCTCTTG	
hunam UBA3	Forward	TGGTGTTGGTGCTTGTAA	NM_001363861.1
	Reverse	GTTGTATGCTTCCTCCTCTAA	

Table S2. Key Resources Table

Reagent type (species) or resource	Designation	Source or reference	Identifiers	Additional information
Cell line (*M. musculus*)	Wild-type and *Dyrk2-/-* MEFs	Yoshida et al., 2020 doi: .org/10.7554/eLife.57381	N/A	
Cell line (*H. sapiens*)	hTert-RPE1	ATCC	Cat# CRL-4000 RRID: CVCL_4388	
Cell line (*H. sapiens*)	DYRK2 -/- hTert-RPE1 (#1, #2)	This study	N/A	
Cell line (*H. sapiens*)	Lx293T	TaKaRa Bio	Cat# 632180 RRID: CVCL_4401	
transfected construct	hunah DYRK2/pEGFP-C1	This study	N/A	
transfected construct	human DYRK2 K251R/pEGFP-C1	This study	N/A	
transfected construct	human NAE1/pcDNA3 FLAG	This study	N/A	
transfected construct	human UBA3/pcDNA3 FLAG	This study	N/A	
transfected construct	HA-Ub/pcDNA3	This study	N/A	
transfected construct	pcDNA3+FLAG	This study	N/A	
biological sample (Adenovirus)	Adenovirus-Cre	Yokoyama-Mashima et al., 2019 doi: 10.1016/j.canlet.2019.02.046.	N/A	
biological sample (Adenovirus)	Adenovirus-human *DYRK2*	Yokoyama-Mashima et al., 2019 doi: 10.1016/j.canlet.2019.02.046.	N/A	
biological sample (Adenovirus)	Adenovirus-human *DYRK2 K250R*	Yokoyama-Mashima et al., 2019 doi: 10.1016/j.canlet.2019.02.046.	N/A	
Antibody	Anti-α tublin (Mouse monoclonal)	Sigma-Aldrich	Cat# T5168, RRID:AB_477579	WB (1:1000)
Antibody	Anti-ATM (Mouse monoclonal)	Santa Cruz Biotechnology	Cat# sc-135663, RRID:AB_2062962	WB (1:300)
Antibody	Anti-ATM (phospho S1981) (Rabbit monoclonal)	abcam	Cat# ab81292, RRID:AB_1640207	WB (1:50000)
Antibody	Anti-CHK2 (Mouse monoclonal)	Santa Cruz Biotechnology	Cat# sc-17747, RRID:AB_627258	WB (1:300)
Antibody	Anti-CHK2(phospho Thr68) (Rabbit monoclonal)	Cell Signaling Technology	Cat# 2197, RRID:AB_2080501	WB (1:1000)
Antibody	Anti-CyclinD1 (Rabbit polyclonal)	Santa Cruz Biotechnology	Cat# sc-753, RRID:AB_2070433	WB (1:500)
Antibody	Anti-DYKDDDDK (Mouse monoclonal)	Transgenic	Cat# KO602, RRID:N/A	ICC (1:125)
Antibody	Anti-DYKDDDDK (Mouse monoclonal)	Sigma-Aldrich	Cat# F3165, RRID:AB_259529	WB (1:4600)
Antibody	Anti-DYRK2 (Rabbit polyclonal)	Sigma-Aldrich	Cat# HPA027230, RRID:AB_1847925	WB (1:1000)
Antibody	Anti-GAPDH (Mouse monoclonal)	Santa Cruz Biotechnology	Cat# sc-32233, RRID:AB_627679	WB (1:3000)
Antibody	Anti-GFP (Rabbit monoclonal)	abcam	Cat# ab183734, RRID:AB_2732027	WB (1:30000)
Antibody	Anti-Histon H3 (gort polyclonall)	Santa Cruz Biotechnology	Cat# sc-8654, RRID:AB_2118303	WB (1:300)
Antibody	Anti-MDM2 (Mouse monoclonal)	Thermo Fisher Scientific	Cat# 33-7100, RRID:AB_2533136	WB (1:1000)
Antibody	Anti-NAE1/APPBP1 (Rabbit monoclonal)	Cell Signaling Technology	Cat# 14321, RRID:AB_2798448	WB (1:1000)
Antibody	Anti-NEDD8 (Rabbit monoclonal)	abcam	Cat# ab81264, RRID:AB_1640720	WB (1:1000)
Antibody	Anti-p21 Waf1/Cip1 (Rabbit monoclonal)	Cell Signaling Technology	Cat# 2947, RRID: AB_823586	WB (1:1000)
Antibody	Anti-p27 (Rabbit polyclonal)	Santa Cruz Biotechnology	Cat# sc-528, RRID:AB_632129	WB (1:300)
Antibody	Anti-p38a MAPK (Mouse monoclonal)	Cell Signaling Technology	Cat# 9217, RRID:AB_331298	WB (1:1000)
Antibody	Anti-p53 (Mouse monoclonal)	Santa Cruz Biotechnology	Cat# sc-126, RRID:AB_628082	WB (1:1000)
Antibody	Anti-phospho-Histone H2A.X(Ser139) (Mouse monoclonal)	Sigma-Aldrich	Cat# 05-636, RRID:AB_309864	ICC (1:300)
Antibody	Anti-phospho-Histone H2A.X(Ser139) (Rabbit monoclonal)	Cell Signaling Technology	Cat# 9718, RRID:AB_2118009	ICC (1:400)
Antibody	Anti-phospho-p53 (ser15) (Rabbit polyclonal)	Cell Signaling Technology	Cat# 9284, RRID:AB_331464	WB (1:1000)
Antibody	Anti-phsopho-p38(Thr180/182) (Rabbit monoclonal)	Cell Signaling Technology	Cat# 9215, RRID:AB_331762	WB (1:1000)
Antibody	Anti-UBA3 (Mouse monoclonal)	Santa Cruz Biotechnology	Cat# sc-377272, RRID:N/A	WB (1:300)
sequence-based reagent	human *DYRK2* siRNA#1	BEX	608481	
sequence-based reagent	human *DYRK2* siRNA#2	ThermoFisher Scientific	HSS112284	
sequence-based reagent	Silencer Select Negative Control (siControl)	ThermoFisher Scientific	4390843	
sequence-based reagent	*human TP53 siTP53#1*	ThermoFisher Scientific	HSS110905	
sequence-based reagent	*human TP53 siTP53#2*	ThermoFisher Scientific	HSS186391	
chemical compound, drug	MG-132	Sigma-Aldrich	474790	
chemical compound, drug	nocodazole	Tocris Bioscience	31430-18-9	
chemical compound, drug	SB203580	Selleck	S1076	
software, algorithm	BZ-X800 Analyzer	Keyence	BZ-X800 Analyzer	
software, algorithm	Excel	Microsoft	Mac2019	
software, algorithm	Flowjo	TOMY DIGITAL BIOLOGY	Flowjo	
software, algorithm	Fusion	M&S Instruments	Fusion	
software, algorithm	GraphPad Prism 7	GraphPad Software Inc.	Mac OS X	
software, algorithm	PikoReal Software 2.1	ThermoFisher Scientific	PikoReal Software 2.1	